Nonlinear Lateral Stiffness and Bearing Capacity of Suction Caissons for Offshore Wind-turbines

by

F. Gelagoti[1,2] , I. Georgiou[3], R. Kourkoulis, and G. Gazetas[3]

A B S T R A C T

The paper investigates the linear-elastic and nonlinear stiffnesses of a suction caisson used as monopod foundation for an Offshore Wind-Turbine (OWT). Starting from caissons at low working stresses, in which case the linear elastic theory provides an adequate engineering model for soil, analytical expressions for the elastic stiffness matrix of a flexible skirted foundation are proposed and validated. To account for the nonlinear foundation response, the paper proposes a simplified equivalent linear iterative approach where the effective foundation stiffness is expressed in terms of deformation amplitude. To this end, utilizing results from a 3D finite element parametric study, non-dimensional charts have been produced for caissons ranging from perfectly rigid to flexible with variable embedment ratios. To deal with uncertainty on the conditions at the soil-skirt interface, three idealized interface scenarios – "*fully-bonded*", "*tensionless*", "*frictionless*" – are implemented. Reduced values of foundation stiffness are computed for a frictionless contact. On the contrary, the impact of a '*tensionless*' interface, whilst trivial in elastic problems, is intensified with progressing soil inelasticity resulting in severely reduced stiffnesses and capacities. Moreover, with increasing relative skirt flexibility, the elastic stiffnesses of deep suction caissons tend to recede substantially, but the rate of stiffness degradation is fairly attenuated.

Keywords: *suction caisson; stiffness; nonlinear response, imperfect interfaces*

[1] *Correspondance to: fanigelagoti@gmail.com*
[2] *Grid Engineers, Athens, Greece*
[3] *National Technical University of Athens, Greece*

1. INTRODUCTION

Suction caissons are widely used in offshore industry with applications ranging from catenary mooring lines (Colliat et al., 1996) and tension leg platforms (Andersen et al., 1993; Clukey et al., 1995) to monopod installations for the foundation of wind-turbines (Houlsby et al., 2006). A suction caisson is essentially a skirt foundation, i.e. a cylindrical shell with an open bottom ("skirts") and a top slab ("lid") During installation, by pumping the water trapped within the caisson after it has touched the seabed, an under-pressure is created inside the skirt compartment, attracting the foundation downwards until the internal soil plug is perfectly "sealed" onto the caisson's lid.

As long as perfectly undrained conditions are assumed (i.e., when soil permeability is low or/and the application of load is transient), the "sealing" is safe; negative excess pore pressure (often referred to as suction) are generated between the underside of the foundation top plate and the soil, preventing the detachment of the caisson from the surrounding soil. In the best documented case — that of a vertically pulled up caisson— as the inner soil plug is uplifted, the outer soil is dragged beneath the bucket, mobilizing a "reverse end bearing" mechanism of augmented resistance (Senders, 2008). Also, increased values of resistance have been reported for horizontally or rotationally displaced perfectly "sealed" caissons. Hence, to numerically model this response, no separation is allowed between the caisson shaft and the soil, while the latter is typically treated as one-phase medium of undrained shear strength s_u (Cho and Bang, 2002; Deng and Carter, 2000; McCarron and Sukumaran 2000; Sender and Kays, 2002; Sukumaran et al., 1999; Supachawarote et al., 2004).

On the other hand, experimental data are questioning the soundness of such an idealized assumption. Randolph et al. (1998) reported centrifuge model tests of suction caissons in normally consolidated silty clay with some evidence of soil-caisson detachment. The latter appeared in the form of a vertically propagating crack along the skirt periphery, but formed only at very large displacements. At that instant a mild but sudden drop at the caisson capacity by about 18% from the peak value was measured. A companion test in lightly over-consolidated soil, showed crack formation immediately (i.e. at much lower vertical displacements), with a clear vertical scarp face behind the caisson. Then again, the experiments of Clukey et al. (2003) and Coffman et al. (2004), conducted in normally consolidated clay, showed no trace of detachment even at large displacements.

Another source of controversy is related to the available soil strength at skirt periphery. Naturally, as the caisson penetrates within the virgin soil, the shear strength of clay along the skirt is reduced to the remoulded shear strength (which is the original strength, $s_{u,o}$ divided by the soil sensitivity S_t). This is further confirmed by several experimental data (House and Randolph, 2001; Andersen and Jostad, 2002; Houlsby et al., 2005a) according to which a reduction coefficient, α, of the order of 0.2 to 0.4 (defined as the measured shear stress along the skirts divided by undrained shear strength of the virgin soil) has been reported. After penetration, there will be a "set-up" and the shear strength of the clay along the skirt wall eventually increases with time due to dissipation of excess pore pressure, increased horizontal normal effective stress, and thixotropy (Andersen and Jostad, 2002). This strength gain however may not be sufficient to bring the shear strength back to its original value. Thus, lower shear resistance at the soil-foundation interface should be considered prudently.

The caisson performance is further complicated when the "undrained" assumption cannot be met. Depending on the loading rate, the bucket dimensions and the permeability of soil, time–dependent response may be triggered which is essentially controlled by seepage flow mechanics (Zdravkovic et al., 2001; Cao et al., 2002; Chen and Randolph, 2007; Gourvenec et al., 2009; Mana et al., 2014; Achmus and Thieken, 2014)

In this paper a suction caisson is used for the foundation of the Offshore Wind-Turbine, of **Fig.1**. Although not yet tested in real-life projects, a growing body of researchers (Byrne and Houlsby, 2003; Ibsen and Brincker, 2004; Zhu et al., 2014; Cox and Bhattacharya, 2017) are suggesting that suction caissons are a "noise-free" and easy-to-install alternative to monopile installations. But even from a purely geotechnical perspective, the implementation of a caisson for the foundation of a wind turbine is meaningful; the increased rotational stiffness/capacity of a large diameter caisson may ideally resist the large overturning moments (M) and shear forces (H) at the base of the turbine, generated by the coupled action of wind and waves.

The objective of this study is to elaborate further on the response of suction caissons under combined H-M loading. With respect to the state-of-the-art (Taiebat and Carter, 2000; Bransby and Yun, 2009; Gourvenec, 2008; Ukritchon et al., 1998; Gourvenec and Barnett, 2011; Barari and Ibsen, 2012; Vulpe, 2015), where attention was drawn to the assessment of bearing mechanisms and the associated development of generalized failure envelopes, this study focuses on the linear-elastic and the nonlinear stiffnesses of the soil-caisson system. Results will be presented in the form of dimensionless graphs allowing a preliminary estimation of foundation deformations. This outcome will expand the work of Doherty et al. (2005) and Liingaard et al. (2007) on the elastic stiffness of flexible skirted foundations, to geometrically nonlinear problems with prevailing soil inelasticity.

2 PROBLEM STATEMENT

A circular suction caisson of diameter D, skirt length L and relative skirt flexibility ($J = \frac{E_{steel}\, t_w}{E_{soil} D}$) is embedded in a uniform deposit of overconsolidated clay (G, s_u). The L/D ratio is varied parametrically to model a very shallow caisson with L/D = 0.2 and two deeper caissons with L/D = 0.5 and L/D = 1.

The skirt thickness (defined by the ratio D/t_w) and the relative skirt flexibility J varies parametrically representing caissons with relatively flexible to rigid skirts. According to Bye et al (1995), Colliat et al (1996), Houlsby et al (2005a), and Foglia et al (2016), the reported diameter to skirt thickness ratios (D/t_w) for steel caissons typically takes values of approximately 350 – 500. For example, for a suction caisson of D=15 m (which is standard for the foundation of medium-sized turbines), following the aforementioned D/t_w recommendation, a skirt thickness of 7.5 mm to 30 mm is estimated. Assuming that the resisting soil is a medium soft clay of undrained shear strength s_u=30-60 kPa and Young's Modulus (at low strains)in the range of 20 -60 MPa, which can be penetrated without the need of internal stiffeners, the parameter J is expected to range between 10-35. In firmer clays, to suppress buckling of the skirt shell during penetration, most suction caissons will include some internal structure, usually consisting of either vertical plates or annular plates, to provide strength and stiffness to the cylindrical shell (Houlsby & Byrne, 2005b). In these cases, J values higher than 35 are anticipated, the skirts can be assumed to be rigid compared to the surrounding soil and the caisson response is pretty much captured by the response of a perfectly rigid caisson.

Moreover, in view of the argument presented previously, it becomes clear that the mechanical behaviour of the soil-caisson interface cannot be known a-priori. Even with undrained conditions, the type of loading and its history, the soil material and the installation method may significantly affect the maximum available resistance at the soil-footing interface. In an attempt to envelope the most probable load-carrying capacity of suction caissons (accounting for a variety of soil-footing interfaces) three generic interaction scenarios are analysed (**Fig. 2**):

(a) An upper-bound scenario in which the caisson is "*fully-bonded*" on the surrounding soil.

(b) *A "tensionless"* scenario allowing separation of the foundation from the surrounding soil when tensile stresses are about to develop, while the inner soil plug remains in full contact with the caisson. This assumption better reflects the appearance of a vertical crack at the caisson periphery in overconsolidated soil deposits. Meanwhile the maximum available shear resistance at the interface equals the undrained soil shear strength (s_u) of the intact soil.

(c) *A "frictionless"* scenario, in which case the interface is completely smooth (offering zero shear resistance), but no detachment is permitted between the soil and the caisson. This is clearly a theoretical scenario deliberately selected to describe the case of a highly remoulded material along the skirt periphery, which cannot sustain a vertical free face to detach from the caisson, but offers negligible frictional resistance. At l rapidly-induced deformations (as those provoked by an intense storm or an earthquake event), suction is expected to be developed at the backside of the caisson (offering tensile capacity that resists to the formation of gap between the caisson shaft and the surrounding soil) thus providing slightly augmented short-term shaft resistance.

It needs to be stressed out that in reality there is no strict discrimination between "*tensionless*" and "*frictionless*" interface scenario. This is essentially a numerical distinction aiming at isolating the effect of each resistance parameter (tangential and normal) to the overall caisson response. Depending on the amplitude of the imposed deformation and the parameters discussed previously, the actual soil-caisson interface behavior may vary between the two theoretical cases. Therefore, for design purposes, it is recommended that the caisson response is estimated on the basis of the most conservative scenario (at any given displacement), instead of committing to one single interface scenario assuming to be applicable for low-amplitude and high-amplitude loadings.

3 FINITE ELEMENT MODEL

The problem is solved numerically using the finite element software ABAQUS (Dassault Systèmes, 2013). The finite element mesh is portrayed in **Fig. 3a** for a shallow caisson (L/D = 0.2). An analogous mesh strategy was adopted for the other two ratios (maintaining a constant discretization along the diameter while adjusting the mesh in the vertical direction). A finer mesh is applied within the depth of the embedment layer (where nonlinearities are more prominent), while mesh coarseness increases away from the foundation.

The boundaries of the semi-cylindrical mesh are positioned sufficiently far to avoid spurious boundary-effects on foundation response: two and a half diameters ($2.5D$) on either side of the foundation for the radial boundaries, and $3D$ beneath the tip of the foundation. For laterally loaded caissons where the soil pressures decay rapidly with depth, a bottom boundary placed at a distance of $3D$ is considered sufficient to simulate halfspace conditions (Poulos and Davis, 1974). Displacement boundary conditions prevent the out-of-plane movement of the vertical face of symmetry as well as the radial horizontal displacement of the circumferential nodes, while the base is fixed in all three directions.

The soil is modelled using eight-node hexahedral continuum elements (C3D8), while the steel foundation (lid and skirts) is simulated with linear elastic shell elements. Special-purpose contact elements of zero thickness (available in ABAQUS) are sandwiched between soil and caisson allowing both sliding (when the prescribed shearing capacity is exhausted) and separation (when net tension is about to develop). By appropriately adjusting the interface description, the aforementioned three interface scenarios are reproduced.

Soil Constitutive model

Warranted by the assumption of fully undrained conditions, the soil is treated as an isotropic homogeneous single-phase medium. The stress-stain bevaviour is described by a simplified kinematic hardening model in the context of Von Mises associative plasticity. The formulation has been implemented as a subroutine in Abaqus and has been parameterized by Gerolymos and Gazetas (2005) and Anastasopoulos et al. (2011) to simulate the nonlinear behaviour of clays under undrained conditions as briefly presented in the ensuing.

The evolution of stress is defined by :

$$\sigma = \sigma_o + a \qquad (1)$$

where σ_o corresponds to the stress at zero plastic strain, and a is a backstress parameter, which determines the center of the yield surface given by the following law:

$$\dot{a} = C \, \frac{1}{\sigma_o} \, (\sigma - \alpha)\dot{e^{pl}} - \gamma \alpha \dot{e^{pl}} \qquad (2)$$

where C the initial kinematic hardening modulus and γ determines the rate of decrease of the kinematic hardening with increasing plastic deformation. At large plastic strains, when σ approaches σ_y , the magnitude of α becomes equal to $\alpha_s = C/\gamma$,$\dot{\alpha}$ tends to zero and

$$\sigma_y = C/\gamma + \sigma_o \tag{3}$$

For clays, the maximum yield stress σ_y is controlled by the undrained shear strength of the material s_u according to Eq. (4) :

$$\sigma_y = \sqrt{3}s_u \tag{4}$$

and the parameter γ may then be defined as :

$$\gamma = \frac{C}{\sqrt{3}s_u - \sigma_o} \tag{5}$$

For the full description of the nonlinear behavior of clay, only three parameters need to be determined: the undrained shear strength s_u, the rigidity index E_{soil}/s_u , and γ. Throughout this study a uniform clay material of s_u = 60 kPa is assumed, while a ratio of E_{soil}/s_u = 1000 and γ = 1667 were found to lead to the best match of the experimentally derived $G:\gamma$ (shear modulus–shear strain) and $\xi:\gamma$ (damping–shear strain) curves provided by Raptakis et al. (2000) as portrayed in **Fig. 3b**.

Despite its simplicity, this 3-parameter constitutive model has been extensively validated in the past against physical model testing demonstrating its effectiveness in describing reasonably well the overall soil-foundation system response (**Fig. 3c**). Indicative examples (relevant to the study presented here) involve the modeling of surface and slightly embedded foundations subjected to cyclic loading and seismic shaking (Anastasopoulos et al., 2011), the cyclic performance of piles and caissons subjected to horizontal/moment loading [Giannakos et al. (2012)] and the seismic response of circular tunnels in clay (Tsinidis et al., 2014; Bilotta et al., 2014).

Validation of the Finite Element Model

The idealized case of a circular skirt foundation (of diameter D) resting in a homogeneous halfspace of undrained shear strength s_u is employed herein as a benchmark problem. The lid of the caisson (which is typically welded with stiffeners) is assumed to behave as rigid, hence the structural flexibility of the caisson is essentially controlled by the flexibility of its skirt. To derive elastic stiffnesses and ultimate bearing loads, the caisson is subjected to controlled displacements in all principal directions. For the computation of the latter a large-strain computation is undertaken updating the stiffness matrix after each loading increment based on the deformed geometry.

In **Fig. 4** the elastic stiffness computation results of this study (derived for fully-bonded contact by applying controlled displacement in one direction while maintaining *zero*-displacement in all others) are compared with the results of Doherty et al. (2005) for suction caissons having either very flexible (t_w=0.02 m) or non-flexible skirts (t_w= 0.2m). Overall, the agreement is quite good. Some deviations may be witnessed in the values of rotational stiffness K_R for L/D > 0.5 probably attributable to differences on solving procedure (finite element against a scaled boundary element method) and the level of mesh refinement.

The adequacy of the proposed finite element methodology to capture the foundation bearing mechanisms and the associated ultimate loads for different loading paths and interface scenarios is confirmed with the published results of Vulpe (2015) and Hung and Kim (2012). In the former case, either translational or rotational displacements (without preventing the foundation from rotating or displacing horizontally) are applied at the Load Reference Point (LRP) which for the sake of this particular comparison only is taken at the bottom middle of the foundation. The estimated horizontal and rotational capacities as a function of the embedment ratio L/D, for two different interface scenarios (i.e. "*fully-bonded*" and "*frictionless*") are portrayed in **Fig. 5a**. For caissons with L/D ≥ 0.2 the comparison is judged as satisfactory. However, for extremely shallow (L/D = 0.1) and "*frictionless*" caissons, the capacity calculations are apparently quite sensitive to the discretization properties at the vicinity of the caisson. As a result, an overprediction (of the order of 15%) is observed compared to the values of Vulpe (which have been produced by an extremely fine mesh). An additional comparison, with LRP at the lid of the caisson is shown in **Fig. 5b**. In this case, our FE simulations are very close to those of Hung and Kim (2012) for all embedment ratios between 0.2 and 1.0.

4 ELASTIC STIFFNESS MATRIX OF A SUCTION CAISSON

In the most general case, when the wind-turbine of **Fig. 1** is subjected to the concurrent action of wind, wave or earthquake loading, a 5 degree-of-freedom loading is transmitted at the top of its foundation. For foundations at low working stresses, linear elastic theory provides an adequate engineering model, and their response is described through:

$$\begin{bmatrix} H_1 \\ H_2 \\ T \\ M_1 \\ M_2 \end{bmatrix} = \begin{bmatrix} 0 & K_H & 0 & 0 & 0 & -K_{RH} \\ 0 & 0 & K_H & 0 & K_{RH} & 0 \\ 0 & 0 & 0 & K_T & 0 & 0 \\ 0 & 0 & K_{RH} & 0 & K_R & 0 \\ 0 & -K_{RH} & 0 & 0 & 0 & K_M \end{bmatrix} \begin{bmatrix} u_1 \\ u_2 \\ \omega \\ \theta_1 \\ \theta_2 \end{bmatrix} \tag{6}$$

Linearity is not unrealistic for over-consolidated clays (as the one of our example problem) that are stressed below their yield limit (Wroth, 1971).

Rigid Suction Caissons

The closed-form expressions presented below have been proposed by Lekkakis (2012) to describe the stiffness of a suction caisson with absolutely rigid shell (i.e. rigid lid and rigid skirts), embedded in a homogeneous halfspace assuming load reference point at the center lid.

$$K_{H,rigid} \approx \frac{8GR}{2-\nu}\left(1 + 1.7\left(\frac{L}{D}\right)^{0.65}\right) \tag{7}$$

$$K_{R,rigid} \approx \frac{8GR^3}{3(1-\nu)}\left[1 + 1.9\frac{L}{D}\ \left(1 + \frac{2\,L}{D}\right)^{1.4}\right] \tag{8}$$

$$K_{RH,rigid} \approx 0.6\ K_H L \tag{9}$$

$$K_{T,rigid} \approx \frac{16}{3}GR^3\left[1 + 5.0\left(\frac{L}{D}\right)^{0.9}\right] \tag{10}$$

Caisson Foundations with Flexible Skirts

The structural flexibility of the cylindrical shell skirts of a suction caisson depends on the relative stiffness of the surrounding soil with respect to the stiffness of the skirts and the geometric parameters D, L, t_w. In dimensionless terms, the stiffness of the flexible caisson (under the condition that the lid is perfectly rigid) may be expressed in terms of the stiffness of the rigid caisson (given by Eq. 7-10), as:

$$\frac{K_i}{K_{i,rigid}} = f\left(\frac{E_{steel}\,t_w}{E_{soil}\,D},\ \frac{L}{D}\right), \quad i = H, R, HR, T \tag{11}$$

in which $J = \frac{E_{steel}\,t_w}{E_{soil}\,D}$ expresses the relative rigidity of the caisson skirts over the soil. **Fig. 6** portrays Eqn (11) for each of the four stiffnesses, K_H , K_R, K_{HR} , K_T. By simply reading the charts, the stiffness of any suction caisson with flexible skirts may be estimated. It is important to note that although the results presented in **Fig.6** represent *fully-bonded* conditions, the very same trends are also applicable to the remaining interface scenarios. Consequently, **Fig. 6** may be used to estimate the reduction on the initial (elastic) stiffness of a caisson (owing to skirt flexibility only) for any interface scenario.

5 NONLINEAR STIFFNESSES: EFFECT OF INTERFACES

The elastic stiffnesses derived so far may sufficiently reproduce the soil-foundation interaction for a wind-turbine under normal wind conditions or under small seismic shaking. During severe storms or strong earthquake excitations the turbine is subjected to intense lateral loading (environmental or inertial) accompanied with excessively high overturning moments on its monopod foundation. These moments are disproportionally large compared to the vertical load of the turbine, triggering a rocking-dominated response; the caisson detaches (at least partially) from the supporting soil transferring increased stressing under the opposite side of the foundation.

'Equivalent-Linear' Stiffness

A detailed analysis of such highly nonlinear soil-foundation interaction problems requires rigorous 3D modelling. Although such analyses have been published in a number of research papers (Hung and Kim, 2012; Kourkoulis et al., 2014; Vulpe, 2015; Penzes et al., 2016; Skau et al., 2017), they are mainly focusing on estimating the ultimate capacity of the foundation ignoring the grey zone covering the transition from "elasticity" to "failure". Computing foundation deformations and soil reactions stemming from nonlinear rocking, is handled herein by exploring the concept of Equivalent-linear stiffness, initially introduced by Figini (2010). By mimicking the familiar concept of equivalent-linear shear modulus to describe nonlinear soil behavior, in this study the nonlinear stiffness of a suction caisson is approximated by an iterative procedure that allows the estimation of the 'effective' foundation stiffness as a function of non-dimensional deformation.

Recently, Gazetas et al. (2013) and Adamidis et al. (2014) utilized theoretical results from nonlinear finite element analyses to develop dimensionless expressions for equivalent-linear static and dynamic rotational stiffness for shallow footings of variable geometry. The material presented here extends the above work to non-rigid circular skirt foundations of $0.2 < L/D < 1$ and all modes of lateral response (R, H, RH). For the cases examined, a zero bearing load condition is assumed (V=0) justified by the very large safety factors against vertical loading — of the order of 10 or even higher (Houlsbly et al., 2006) — that are commonly encountered in reality.

Dimensional Analysis of a Suction Caisson in a yielding soil

The maximum horizontal (H) or rotational (M) load-carrying capacity of a typical suction caisson (in the most general case that of a 'tensionless' interface scenario) is a function of nine independent variables (assuming a perfectly rigid cap and zero vertical load V):

$$H\ (or\ M) = f\ (D, L, E_{soil,} E_{steel}, s_u, t_w, \gamma, u\ (or\ \theta)) \qquad (12)$$

In **Eq.12** the nine variables H = [M][L]/[T^2], D = [L], L = [L], E_{soil} = [M]/[T^2][L] , E_{steel} = [M]/[T^2][L], s_u = [M]/[T^2][L], t_w = [L], γ = [M]/[T^2][L^2], u = [L] involve three independent reference dimensions (r=3), that of mass [M], length [L], and time [T]. According to the Vaschy (1892)-Buckingham (1912) π-theorem the number of independent dimensionless Π-products is equal to the number of physical variables appearing in **Eq. (12)** (nine variables) minus the number of reference dimensions (three). Therefore, for the dimensionless description of the problem we need 6 Π-terms. These are:

- the embedment ratio **L/D** of the caisson
- the dimensionless horizontal capacity $4H/s_u\pi\, D^2$ appearing in the ensuing as $\boldsymbol{H/As_u}$ (with A being the plan view of the caisson)
- the relative rigidity parameter $\boldsymbol{J = \frac{E_{steel}\, t_w}{E_{soil}\, D}}$
- the soil rigidity ratio of the yielding soil $\boldsymbol{E_{soil}/s_u}$
- the stability parameter $\boldsymbol{s_u/\gamma' L}$
- and the dimensionless displacement $\boldsymbol{u/D}$

With the six Π-terms established, Eq. 12 reduces to :

$$H/As_u = f\ (\tfrac{L}{D}, J, E_{soil}/s_u\,,\ s_u/\gamma' L\,,\ u/D) \qquad (13)$$

In the case of '*perfectly-bonded*' or '*frictionless*' interface conditions, where the foundation soil is assumed to be always in contact with the caisson, the stability parameter has no physical meaning and may be omitted from the dimensional formulation. Thereby, the results of the next paragraphs are generally applicable for any $s_u/\gamma' L$ unless specifically stated otherwise.

A schematic representation of the dimensional formulation described above is provided in **Fig. 7** for "frictionless" and "tensionless" interface scenarios. The demonstration example involves four caissons with diameters ranging from D = 5 m to D = 20 m embedded into clay profiles of varying s_u (s_u =45 kPa-240 kPa). It may be easily observed that the response of any suction caisson configuration (described by a given set of dimensionless Π-terms) may be expressed by a unique dimensionless load-displacement curve.

Comment on the stability parameter $s_u/\gamma' L$

The stability parameter $s_u/\gamma' L$ is introduced into the dimensionless formulation to account for the contribution of the detached soil face (lying oppositely to the loading direction) to the overall load-carrying mechanism of the caisson. Its effect is schematically outlined in the snapshots of **Fig. 8** illustrating distribution of plastic deformations and shear stressing along the skirts of the caisson at a characteristic loading instant (i.e. at u/D=0.02). Depending on the amplitude of $s_u/\gamma' L$, two distinctively different states of response may be recognized. The first one, denoted herein as 'stable' state is achieved for relatively high $s_u/\gamma' L$ ratios. At this state, as the caisson moves rightwards, the soil lying behind its leeward side is completely separated from it, forming a clear vertical gap that spreads along the entire skirt length. As the caisson is pushed further to the right, the area of soil-caisson detachment is expanding, and eventually (when the ultimate horizontal capacity is attained) more than half the caisson periphery appears to be completely inactive (i.e. white areas in the contour plots of **Fig 8a**.). This type of response is associated with reduced capacity values as depicted in the plots **Fig 8d** (thin black line). On the other hand, when the stability parameter is low (e.g. $s_u/\gamma' L$ = 0.1-0.3 for caissons with L/D= 1), the detached soil fails under its self weight. As a result, the gap is shallower, while larger amount of soil remains in contact with the caisson (**Fig. 8b**). The latter contributes to the overall capacity resulting in augmented resistance values (**Fig 8d** – bold black line).

The effect of $s_u/\gamma' L$ Π-term on the dimensionless stiffness and capacity of caissons is nicely captured in the plots of **Fig 8c-f**. Shallow caissons (with L/D = 0.2) are treated separately from deeply embedded caissons of (L/D = 1), and for each embedment ratio five caissons are analysed (having all Π-terms identical except the stability term $s_u/\gamma' L$). It is important to observe that while the effect of $s_u/\gamma' L$ term is particularly important for deeply embedded caissons (**Figs 8d and f**), it appears to be trivial for caissons with L/D = 0.2 where it may be safely ignored (**Figs 8c and e**).

6 PRESENTATION OF RESULTS: EFFECT OF INTERFACE BEHAVIOUR

Results are obtained for massless skirted footings of L/D = 0.2, 0.5, 1 subjected to horizontal displacements or rotations of gradually increasing amplitude. By recording the variation of resisting force or moment with imposed displacement or rotation the stiffness degradation charts of **Fig. 9a**, **10a** and **13** are developed. The respective load-carrying curves presented in the form of dimensionless P-δ or M-θ curves are also provided in **Figs. 9b and 11b** for the three theoretical soil–foundation interface scenarios discussed previously: "*fully-bonded*", "*frictionless*" and "*tensionless*" contact. In the first set of analyses, a perfectly rigid skirted footing is assumed embedded within a uniform inelastic soil of E_{soil}/s_u = 1000. The effect of soil rigidity and skirt flexibility is introduced in the sequel (in **Figs. 14-17**).

Horizontal Translation (imposing u with θ=0)**.** The representation of K_H^{NL} as a function of the dimensionless lateral displacement u/D is portrayed in the charts of **Fig. 9** in logarithmic-natural scale. In each chart, three separate curves are plotted, one for each of the contact scenarios analysed. For ease of reference, all stiffness terms have been divided by the elastic stiffness K_H. For small u/D values (i.e., $u/D < 10^{-4}$), the soil behaves almost elastically and the effective horizontal stiffness (for '*fully-bonded*' conditions) equals the elastic stiffness K_H (derived previously). As the u/D increases, soil yielding prevails and the foundation stiffness drops at an increasing rate. Accordingly, three regions of distinctive performance may be recognized:

- a "*quasi-elastic*" region where $K_H^{NL} \approx \ K_H(0)$
- a "*failure-region*", typically appearing for u/D > 0.01. The foundation performance at that stage is better captured by the plots of **Fig. 9b**.
- an "*intermediate region*" covering the space in-between.

As we deviate from "*fully-bonded*" conditions, the initial foundation stiffness (at u/D=0) also deviates from its elastic value K_H. Quite interestingly, the drop (almost irrespectively of L/D) is much higher when a frictionless contact is assumed ($K_H^{fl}\ (0) \approx 0.8\ K_H$) compared to the minimal drop invoked by the tensionless contact ($K_H^{tl}\ (0) \approx 0.92\ K_H$).

A conceptual explanation is attempted with the sketch of **Fig. 10** where the cylindrical volume of the skirted foundation has been replaced by a circumscribed cuboid comprising five surfaces: the square lid (denoted as side (1)) and four rectangular sides with plan view $D\ x\ L$ (sides (2) –(5)).

Under "*fully-bonded*" conditions, resistance to the horizontal movement of this hypothetical cuboid is offered by all five sides: sides (1), (2) and (4) react to the imposed movement through shearing, while sides (3) and (5) transmit normal stresses to the soil. In case of a frictionless interface, the contribution to resistance offered from sides (2) and (4) is completely canceled, resulting in a 20% drop in stiffness compared to the "*fully-bonded*" case. On the other hand, under the assumption of a tensionless contact, only side (3) (lying opposite to the direction of loading) detaches from soil and does not contribute to the overall foundation resistance. This results in a maximum loss in stiffness of a mere 10% for the shallow caisson, while this value drops further as the L/D ratio increases.

This trend is reversed, when comparing the two imperfect contact-scenarios in terms of ultimate capacity. In case of a tensionless interface, a clear gap is expected to form on the backside opposite to the direction of loading, completely cancelling the development of active soil prism conditions. The loss of resistance at the rear sidewall appears to be higher than the maximum mobilized shearing resistance at the two parallel sidewalls (that remain inactive in the "*frictionless*" scenario), resulting eventually in lower capacity values when a tensionless contact is assumed.

Rotation (imposing rotation θ with $u = 0$)**.** Skirted footings subjected to purely rotational deformations show increased sensitivity to imperfect contact-scenarios (**Fig. 11**). The rotational movement may be decomposed to a rotation of the foundation lid, a torsional movement of sides (2) and (4) (of the approximate model of **Fig. 10**) that mobilize soil shearing, and a coupled rocking-translational movement of sides (3) and (5) producing normal and shear stressing. Consequently, when a frictionless boundary is activated, the contribution of sides (2) and (4) to the total foundation stiffness is completely annulled, while on top of this an attenuated participation of sides (3) and (5) is expected. Under these conditions the frictionless rotational stiffness K_R decreases by 30% (almost uniformly for all L/D ratios) with respect to the rotational stiffness attained at perfectly elastic conditions. Once again, the foundation stiffness is less affected by the tensionless interface: a mere 10% drop is observed.

The effect of interface behaviour on ultimate moment capacity of skirted footings is portrayed in **Fig. 11b and Fig. 12**. Similar to horizontal loading, there is a reversal in the trend and the decrease in capacity is normally more pronounced when a tensionless interaction is assumed. For this particular case, resistance to the applied rotation is offered through shearing at the front side of the foundation (i.e. the one following the direction of loading) followed by an abruptly terminated scoop mechanism (which does not evolve all the way upwards to reach the soil surface due to the gap generation at the back of the caisson). This is not accurate for shallow caissons (L/D = 0.2), where the loss in foundation capacity for either imperfect contact scenario is equal to 15 %. As may easily be witnessed by the plots of **Fig. 12a** when the confinement is low, the rotational capacity, for both interface scenarios, is controlled by the formation of almost identical shallow scoop mechanisms, accompanied by an inverted ellipsoidal scoop within the encased soil identified in the literature by the name “retina” (Kourkoulis et al., 2014). Moreover, the resistance offered along the shallow peripheral shell (which is inevitably affected by the interface scenario assumed) is only a small percentage of the ultimate resistance, explaining the almost identical behavior between a “*tensionless*” and a “*frictionless*” caisson.

Coupled swaying-rocking stiffness. When a purely horizontal force is applied at the top of a skirted foundation, the resulting displacement will involve rotation as well as translation. To account for this coupling effect (which becomes more pronounced with increasing embedment) the swaying-rocking stiffness K_{HR}^{NL} needs to be derived. The latter is the ratio of the Moment reaction (M) of a footing subjected to purely horizontal displacement over the imposed displacement u, when the rotational movement is restrained ($u \neq 0, \theta = 0$). Results on the nonlinear response of K_{HR}^{NL} for the three L/D ratios are portrayed in **Fig. 13**. As with the previous stiffnesses, the assumption of imperfect interface conditions (*frictionless* or *tensionless*) reduces the available resistance along the skirts of the caisson and thereby the amplitude of the ratio K_{RH}^{NL} / K_{RH}. The only outlier to this rather predictable pattern is the response associated with a “*frictionless*” footing with L/D equal to 0.2. In this particular case, the K_{RH}^{NL} / K_{RH} ratio is greater than unity, suggesting that the moment developed due to the restrained rotation of the caisson exceeds even the moment of the “*fully-bonded*” case. This simply reflects the fact that if a very shallow caisson was subjected to horizontal loading and no friction could be developed along its skirts, it would essentially tend to rotate rather than displace. Any attempt to restrain this rotation inevitably produces a significant parasitic moment that exceeds the restraining moment of the “*fully-bonded*” case.

Effect of Rigidity Index E_{soil}/s_u on Equivalent Linear Stiffnesses

In the preceding section, analyses were referring to skirted footings embedded within a uniform stratum of typical soft clay material with a rigidity index of E_{soil}/s_u = 1000. In this section, graphs for the nonlinear rocking stiffness are also provided for softer and stiffer sites: E_{soil}/s_u = 500 and E_{soil}/s_u= 2000. In all scenarios analysed, the dimensionless parameter J was fixed at a very high value (J >1000) to ensure that the skirted foundation will continue to behave as practically rigid irrespectively of soil stiffness.

For the sake of brevity, the graphs of **Fig. 14** provide results for shallowly embedded caissons (L/D = 0.2), since it was found that the trends are similar for larger depths of embedment. It is evident that as the rigidity index increases, the left boundary of the intermediate region (where foundation stiffness starts deviating from its initial elastic value) is moving to the left. Due to increased soil stiffness, foundation non-linearity is now triggered at slightly smaller displacements. For example, referring to the horizontal stiffness at "*fully-bonded*" contact (black thick lines in **Fig. 14**), non-linearity takes effect at $u_s^{2000} \approx 3x10^{-5}$ when E_{soil}/s_u = 2000, while a 3.3 higher displacement of $u_s^{500} \approx 10^{-4}$ is required with E_{soil}/s_u = 500.

Apart from that, the rate or shape of stiffness degradation remains almost unaffected by soil rigidity: by simply shifting the original curve to the left (to match the triggering displacement u_s/D or rotation θ_s), curves of variable E_{soil}/s_u may be developed. Hence, it is possible to eliminate the effect of 'rigidity index' and derive unique (non-dimensional) graphs using the following new dimensionless displacement/rotation parameter:

$$u_s = \frac{1000}{E_{soil}/s_u} D \qquad (14)$$

$$\theta_s = \frac{1000}{E_{soil}/s_u} \qquad (15)$$

The doubly normalized curves are presented in **Fig. 15.**

Effect of Skirt Flexibility on Nonlinear Stiffness

The role of skirt flexibility (expressed in terms of the dimensionless parameter J) is summarized in **Fig**. **16** and **Fig. 17.** Parameter J varies from 3.5 – 35. The J = 35 case is selected to represent a steel caisson with a D/t_w in the range of 200 -500 (having no internal stiffeners along its skirts) embedded within a soft to moderately soft clay profile. The J = 3.5 case (representing a quite flexible caisson that is not commonly encountered in real life projects) essentially serves as a theoretical lower-bound that helps to better illustrate the mechanics. Results for J =1000 are also provided representing the upper-bound of a perfectly rigid caisson.

The non-linear caisson stiffnesses are expressed in the form of dimensionless graphs for shallowly (L/D = 0.2) and deeply embedded caissons (L/D = 1) narrowed for the sake of clarity within a range of dimensionless displacement/rotation 10^{-5}< [u/u_s , θ/θ_s.]< 10^{-1}. By normalizing results to their respective elastic stiffness (estimated for a given J and specific interface scenario), it is possible to isolate the effect of skirt flexibility on the stiffness degradation of the caisson.

Characteristic test cases are presented in **Fig.16** referring to a caisson with L/D =1 allowing either a *fully-bonded* or a *frictionless* interface scenario. Clearly, the nonlinear stiffness curves for the caisson with $J = 35$ are almost identical to those of a caisson with J $= 1000$. Therefore, for design purposes it is reasonable to treat caissons with $J > 35$ as practically rigid.

The nonlinear stiffness of relatively flexible caissons (having $J < 35$) may be extracted from the graphs of **Fig.17**. For shallow caissons (with L/D =0.2) the effect of skirt flexibility is less pronounced while it appears to be related to the mechanical properties of the soil-caisson interface. As L/D increases, skirt flexibility is becoming the controlling factor and its effect may be described by a unique trend (pertinent to all three interface scenarios): as J reduces higher displacements have to be imposed to drive the foundation beyond its '*quasi-elastic*' region, while the rate of stiffness degradation (with increasing dimensionless displacement/rotation) decreases.

7 NUMERICAL EXAMPLE

A simple numerical example demonstrates the applicability of the developed graphs to preliminarily analyse suction caissons. Consider the 3.5 MW offshore wind-turbine of **Fig. 1** installed in a uniform stratum of slightly overconsolidated clay (with undrained shear strength (s_u) of 60 kPa and elastic Young's Modulus (E_{soil}) of 60 MPa). According to the IEC61400-3 and Germanischer Lloyd recommendations, at ULS (Ultimate Limit State) conditions the wind-tower is subjected to gale winds of 25 m/s generating a (quasi-static) horizontal wind loading of 1.5 MN acting at nacelle level (i.e at 80m above ground). Moreover, sea waves are creating an additional shear of 2.5 MN at a height of 10 m above ground. Hence, the wind-turbine foundation (which in our example problem is a monopod suction caisson) should be designed to withstand an overturning moment (M) of 145 MNm and a horizontal load (H) of 4 MN. As may be easily confirmed by applying a Limit State Design (LSD) approach, this specific loading may be safely undertaken by (at least) two alternative foundation solutions: a shallow caisson with D = 20 m, L = 4 m and t_w= 12.5 cm (denoted as Caisson 1) and a much deeper caisson with D = 12m, L = 12 m and t_w=12.5 cm

(Caisson 2). Note that the two alternatives are almost equivalent in terms of ultimate strength, with a moment capacity double the ULS Design Moment (of 145 MN). The Factor of Safety (FoS) against overturning moment for the shallow caisson is 2.0, while for the deeper solution the FoS increases to 2.8 (**Table 1**).

Such a limit state approach, although valuable for a preliminary design, provides no evidence on the performance of the caissons under the prescribed loading. Estimation of (inelastic) deformations is possible with the formulas and charts of the paper. Applying a simple iterative procedure, the two caissons are being compared considering two alternative contact scenarios: an optimistic that assumes "*fully-bonded*" interface, and the conservative scenario of a "*frictionless*" contact. The procedure starts with the estimation of *elastic* stiffnesses (K_H, K_R, K_{HR}) of the skirted footings. Combining **Eq. 8-10** with the graphs of **Fig. 6** for a skirt relative rigidity J equal to 22 we estimate for Caisson 1:

K_H = 1654 MN/m, K_R = 166342 MNm/rad and K_{HR} = 3650 MN/rad

For an overturning moment of M = 145 MNm and a horizontal load of H = 4 MN a first estimate on the attained foundation displacement may be derived. That is :

$$\theta_0 = \frac{K_H}{K_H K_R - {K_{HR}}^2} M + \frac{K_{HR}}{K_H K_R - {K_{HR}}^2} H = 0.97\, mrad \quad u_0 = \frac{H}{K_H} + \frac{K_{HR}}{K_H} \theta_0 = 0.0046\, m$$

and in non-dimensional terms θ_o/θ_S = 0.97 x 10^{-3} and u_o/u_S = 0.23 x 10^{-3}

Next, using the graphs of **Fig. 17**, interpolating between the black dashed line that refers to $J = 3.5$ and the black continuous line for $J = 35$, it is possible to estimate the effective foundation stiffness (for $J = 22$) that applies at that particular level of u/u_S and θ/θ_S. In our example a drop of around 80% (on the initial purely elastic values of K) is suggested resulting to an effective stiffness of :

$K^{NL}_{H,1^{st}trial}$= 1488 MN/m, $K^{NL}_{R,1^{st}trial}$= 117271 MN/m and $K^{NL}_{RH,1^{st}trial}$= 2628MN/rad

For these values, the updated foundation displacements are $\theta_{1^{st}\,trial}$ ≈ 1.35 mrad and $u_{1^{st}\,trial}$≈ 0.51 cm.

Proceeding to the 2nd iteration, the foundation stiffness is further reduced to :

$K^{NL}_{H,2^{nd}trial}$= 1455 MN/m, $K^{NL}_{R,2^{nd}trial}$ ≈ 106459 MNm/rad and $K^{NL}_{HR,2^{nd}trial}$ ≈ 2445 MN/rad while the foundation deformations start converging to a slightly increased value of $\theta_{2^{nd}\,trial}$= 1.48 mrad and $u_{2^{nd}\,trial}$≈ 0.52 cm. At the instant, the estimated error is 10 % for the rotation and 3.3% for the displacement. To fall below a 10% error a 3rd iteration is conducted which eventually yields a foundation rotation of θ^{NL} = 1.50 mrad and u^{NL} = 0.53 cm. By applying the same iterative procedure to the Caisson 2 we compute θ^{NL} = 2.7 mrad and u^{NL} = 2 cm.

A detailed comparison on the performance of the two Caissons is presented in **Table 2a,** while in **Table 2b** results corresponding to the "*frictionless*" scenario are presented. Note that, in order to obtain an estimate on the initial elastic stiffness of a non-rigid caisson assuming "*frictionless*" soil-caisson interface, it requires combination of the information provided in **Figs. 9,11, and 13** (i.e. by reading the value on the vertical axis it is possible to estimate the effect of imperfect interface on the initial stiffness value for a perfectly rigid caisson) and **Fig. 6** which provides information on the effect of J on the initial stiffness value (irrespectively of the interface assumption).

The following preliminary remarks may be derived:

- The 'actual' foundation displacements (at ULS state) would have been overly under-predicted by assuming liner-elastic footing response. Even for the "*fully-bonded*" contact, the actual error may be as high as 50%, while with a "*frictionless*" interface the error escalates to 60%.
- Despite the higher FoS, it is the deeper Caisson that displaces the most. Evidently, the larger diameter caisson leads to a rather superior performance and is thus better suited for the monopod foundation of the Wind-tower, where the governing loading is the severely high overturning moment.
- An imperfect contact results in increased foundation displacements/rotations. This increase is of the order of 70% in rotation and 112% in horizontal displacement for Caisson 1, while the deeper alternative (Caisson 2) is slightly more affected (116% and 123% respectively).
- Both Caissons are judged appropriate for the foundation of the example Wind-turbine. In all cases, the maximum rotation lies below 8.7 mrad (which is the maximum allowable rotation for ULS conditions according to DNV2001 standards).

8 CONCLUSIONS

The paper presented expressions and charts for the linear-elastic and the nonlinear stiffness matrix of a flexible suction caisson serving as a monopod footing for an offshore wind-turbine tower. Ultimate capacities for three loading paths were also presented. The results were obtained with 3D finite element models verified against solutions from the literature.

The nonlinear soil-foundation response was handled approximately through a simplified equivalent linear iterative approach where foundation stiffness decreases with deformation amplitude. To this end, non-dimensional charts were developed applicable to flexible caissons with embedment ratios L/D = 0.2, 0.5 and 1.

A significant amount of effort was devoted into exploring the non-trivial role of the soil-sidewalls interface on the rocking response of suction caissons. To this end, three idealized interaction scenarios were assumed: (a) an upper-bound scenario in which the caisson was "*fully-bonded*" on the surrounding soil; (b) a "*tensionless*" scenario allowing separation of the foundation from the surrounding soil and (c) a "*frictionless*" scenario, assuming that the interface was completely smooth, representing cases of excessively remoulded material along the skirt periphery.

It was concluded that both stiffnesses and ultimate capacities of a suction caisson (experiencing combined H-M loading) were affected by the contact conditions at the soil-foundation interface. Elastic stiffnesses were more influenced by a *frictionless* contact, while the effect of a *tensionless* contact (which was found to be trivial in elastic problems) was intensified as soil inelasticity prevails.

Other parameters affecting the non-linear stiffness of a suction caisson was soil rigidity E_{soil}/s_u and skirt relative rigidity J. As soil rigidity index increases, the effective stiffness of a caisson (with respect to its elastic value) at a prescribed displacement/rotation decreases. However, it was possible to eliminate the effect of the latter and derive unique (double-dimensional) stiffness curves by simply expressing them with respect to the dimensionless displacement/rotation parameter u/u_s or θ/θ_s.

The effect of skirt relative rigidity J on the non-linear foundation stiffness was far more complicated. Shallow caissons were the least affected, while on the contrary the non-linear stiffness of a caisson with the $L/D = 1$ was essentially controlled by the flexibility of its skirt especially when imperfect interface conditions were assumed.

Finally, the proposed iterative procedure was demonstrated through a simple numerical example where two caisson alternatives were comparatively assessed. By estimating inelastic deformations at the base of an example OWT, it was concluded that the larger diameter caisson (despite having lower overturning capacity than the deeper alternative) generated lower rotation and displacements, and thus was better suited for the monopod foundation of the example wind-tower. Unsurprisingly, the assumption of a "*frictionless*" contact had an intense effect on the amplitude of the accumulated deformation; the increase in rotation was in order of 70% (for the less sensitive shallow installation), while if a deep caisson was selected, the rotation attained was double the rotation of the "*fully-bonded*" contact.

9 NOTATION

R	Suction Caisson Radius
D	Suction Caisson Diameter
L	Suction Caisson Embedment Length
E_{soil}	Soil Young's modulus
E_{steel}	Steel Young's modulus
t_w	Thickness of the caisson skirt
J	skirt relative rigidity
σ	soil stress
σ_0	soil stress at zero plastic strain
σ_y	maximum yield soil stress
γ	parameter for the definition of non-linear kinematic hardening
a	backstress parameter
C	Initial kinematic hardening
e^{pl}	soil plastic strain
s_u	undrained shear strength of clay
H	horizontal load
M	Moment load
T	Torsion load
u	Horizontal displacement of the foundation
θ	Foundation Rotation
ω	Torsional foundation Rotation

K_i $(i = H, R, HR, T)$ Elastic Stiffnesses

$K_{i,rigid}$ $(i = H, R, HR, T)$ Elastic Stiffnesses assuming rigid caisson

K_i^{fl} $(i = H, R, HR, T)$ Caisson Stiffnesses assuming frictionless contact

K_i^{tl} $(i = H, R, HR, T)$ Caisson Stiffnesses assuming tensionless contact

K_i^{NL} $(i = H, R, HR, T)$ Nonlinear Caisson Stiffnesses

θ_s Dimensionless foundation rotation

u_s Dimensionless horizontal displacement

10 ACKNOWLEDGEMENT

This research study has been financially supported by the Greek State Scholarship Foundation (IKY Fellowships of Excellence for Postdoctoral Studies in Greece -MIS 5001552.

11 REFERENCES

Abaqus, 2013. Standard user’s manual, Abaqus 6.13. Providence, RI, USA: Dassault Systemes Simulia Corp.

Achmus, M., and Thieken, K., 2014. Numerical Simulation of the Tensile Resistance of Suction Buckets in Sand. Journal of Ocean and Wind Energy, 1(4), 231–239.

Adamidis O., Gazetas G., Anastasopoulos I., Argyrou Ch., 2014. Equivalent- Linear Stiffness and Damping in Rocking of Circular and Strip Foundations. Bulletin of Earthquake Engineering, 12(3), 1177-1200.

Anastasopoulos I., Gelagoti F., Kourkoulis R., Gazetas G., 2011. Simplified Constitutive Model for Simulation of Cyclic Response of Shallow Foundations: Validation against Laboratory Tests. Journal of Geotechnical & Geoenvironmental Engineering (ASCE), 137(12).

Andersen, K.H., Dyvik, R., Schroder, K., Hansteen, O.E., Bysveen, S., 1993. Field tests of anchors in clay II: predictions and Interpretation. J. Geotech. Engng, 119, No. 10, 1532–1549.137(12), 1154-1168.

Andersen, K.H., Jostad, H.P., 2002. Shear strength along outside wall of suction anchors in clay. Proceedings of the 31st offshore tenchnology conference, Houston. Paper OTC 10824.

Aubeny, C.P., Moon, S.K., Murff, J.D., 2001. Lateral undrained resistance of suction caisson anchors. International Journal of Offshore and Polar Engineering, 11 (2), 95–103.

Barari, A., Ibsen, L.B., 2012. Undrained response of bucket foundations to moment loading. Appl. Ocean Res. 36, 12-21.

Bye, A., Erbrich, C. Rognlien, B., Tjelta, T. I. 1995. Geotechnical Design of Bucket Foundations, DOI: 10.4043/7793-MS

Bransby, M.F., Yun, G.J., 2009. The undrained capacity of skirted strip foundations under combined loading. Geotechnique 59(2), 115-125,

Bilotta, E., Lanzano, G., Madabhushi, S.P.G., Silvestri, F., 2014. A numerical round robin on tunnels under seismic actions. Acta Geotechnica 9(4), 563–579.

Byrne, B.W., Houlsby, G.T., 2003. Foundations for offshore wind turbines. Phil. Trans. R. Soc. London Ser. A 361, 2909–2930.

Buckingham, E., 1912. On Physically Similar Systems; Illustrations of the Use of Dimensional Equations, Phys. Rev. 4, 345

Cao, J., Phillips, R., Popescu, R., Audibert, J.M.E., and Al-Khafaji, Z., 2002. Numerical Analysis of the Behavior of Suction Caissons in Clay. Proc 12th Int Offshore Polar Eng Conf, Kitakyushu, Japan, ISOPE, 2, 795–799.

Chen, W., Randolph, M.F., 2007. External radial stress changes and axial capacity for suction caissons in soft clay, Géotechnique 57(6), 499–511.

Cho, Y., Bang, S., 2002. Inclined loading capacity of suction piles. Proc. of the 12th International Offshore and Polar Engineering Conference, pp. 827-832.

Clukey, E.C., Morrison, M.J., Garnier, J. and Corte, J.F., 1995. The response of suction caissons in normally consolidated clays to cyclic TLP loading conditions. Proc. Offshore Technology Conf., Houston, OTC 7796.

Clukey, E.C., Aubeny C.P. and Murff J., 2003. Comparison of Analytical and Centrifuge Model Tests for Suction Caissons Subjected to Combined Loads. International Conference on Offshore Mechanics and Arctic Engineering, Volume 3: Materials Technology; Ocean

Engineering; Polar and Arctic Sciences and Technology; Workshops, pp. 889-894, Cancun, Mexico.

Coffman, R.A., El-Sherbiny, R.M., Rauch, A.F., Olson, R.E., 2004. Measured Horizontal Capacity of Suction Caissons. Proc., Offshore Tech. Conf., Houston, Paper 16161.

Colliat, J.L., Boisard, P., Gramet, J.C., Sparrevik, P., 1996. Design and installation of suction anchor piles at a soft clay site in the Gulf of Guinea. Paper OTC 8150, Offshore Technology Conference, Houston, Texas.

Cox, J. A., Bhattacharya, S., 2017. Serviceability of suction caisson founded offshore structures. Proceedings of the Institution of Civil Engineers. Geotechnical Engineering (170), Issue GE3, pp. 273–284.

Deng, W., Carter, J.P., 2000. A theoretical study of the vertical uplift capacity of suction caissons. Proc. 10th Int.Offshore and Polar Engineering Conference, pp. 342-349.

DNV, 1992 Classification Notes No. 30.4, Foundations.Det Norske Veritas, Oslo, Norway.

DNV, 2001. Guidelines for design of wind turbines. Copenhagen, Denmark: Det Norske Veritas.

Doherty, J.P., Houlsby, G.T., Deeks, A. J., 2005. Stiffness of flexible caisson foundations embedded in nonhomogeneous elastic soil. Journal of Geotechnical and Geoenvironmental Engineering, ASCE 131(12), 1498-1508.

Figini, R., 2010. Nonlinear dynamic soil–structure interaction: application to seismic analysis of structures on shallow foundations. Doctoral Disertation, Politecnico di Milano.

Foglia, A., L. B., Ibsen, 2016. Monopod Bucket Foundations Under Cyclic Lateral Loading, International Journal of Offshore and Polar Engineering, 26(2), 109-115.

Gazetas, G., Anastasopoulos, I., Adamidis, O., Kontoroupi, T., 2013. Nonlinear rocking stiffness of foundations. Soil Dynamics and Earthquake Engineering 47, 83–91.

Gazetas, G., 1991. Formulas and charts for impedances of surface and embedded foundations. Journal of Geotechnical Engineering, ASCE 117(9), 1129–1141.

GermanisCher Lloyd Wind Energie, 2005. Guideline for the Certification of Offshore Wind Turbines.

Gerolymos, N., Zafeirakos, A., Karapiperis, K., 2015. Generalized failure envelope for caisson foundations in cohesive soil: static and dynamic loading. Soil Dynamics Earthquake Engng 78, 154–174.

Gerolymos N., Gazetas G., 2005. Nonlinear Lateral Response of Caisson Foundations. Proceedings of the 1st Greece-Japan Workshop on Seismic Design, Observation, Retrofit of Foundations, Athens, Greece, pp. 125.

Giannakos, S., Gerolymos, N. & Gazetas, G., 2012. Cyclic lateral response of piles in dry sand: Finite element modeling and validation. Comput. Geotech. 44, 116–131.

Gourvenec, S., 2008. Effect of embedment on the undrained capacity of shallow foundations under general loading, Geotechnique 58, No. 3, 177–185.

Gourvenec, S., Acosta-Martinez, H.E., Randolph, M.F., 2009. Experimental study of uplift resistance of shallow skirted foundations in clay under transient and sustained concentric loading. Géotechnique 59(6), 525–537.

Gourvenec, S. and Barnett, S., 2011. Undrained failure envelope for skirted foundations under general loading. Geotechnique 61(3), 263-270.

Gourvenec, S. and Mana, D.S.K., 2011. Undrained vertical bearing capacity factors for shallow foundations Geotechnique Letters 1, 101–108.

Houlsby, G.T., Kelly, R.B., Huxtable, J., Byrne, B.W., 2005a. Field trials of suction caissons in clay for offshore wind turbine foundations. Géotechnique 55(4), 287–296.

Houlsby, G.T., Byrne, B.W., 2005b. Design procedures for installation of suction caissons in clay and other materials. Proceedings of the ICE - Geotechnical Engineering 158, 75 - 82.

Houlsby, G.T., Kelly, R.B., Huxtable, J., Byrne, B.W., 2006. Field trials of suction caissons in sand for offshore wind turbine foundations. Geotechnique 56(1), 3–10

House, A.R., Randolph, M.F., 2001. Installation and pull-out capacity of stiffened suction caissons in cohesive sediments. Proceedings of the 11th International Offshore and Polar Engineering Conference, Stravanger, Norway, vol.2. Mountain View, CA, USA: International Society of Offshore and Polar Engineers (ISOPE).

Hung, L.C., Kim, S.R., 2012. Evaluation of Vertical and Horizontal Bearing Capacities of Bucket Foundations in Clay. Ocean Engineering 52, 75–82.

Ibsen L.B., Brincker R., 2004. Design of a new foundation for offshore wind turbines. Proceedings of the 22nd International Modal Analysis Conference (IMAC XXII), Detroit, MI, USA.

IEC (International Electrotechnical Commission),2005. IEC 61400-1: Wind turbines – Part 1: design requirements. Geneva, Switzerland: IEC

Kourkoulis, R.S., Lekkakis, P.C., Gelagoti, F.M., Kaynia, A.M., 2014. Suction caisson foundations for offshore wind turbines subjected to wave and earthquake loading: effect of soil-foundation interface. Geotechnique 64(3), 171-185.

Lekkakis, P., 2012. Analysis of Skirted Foundations for Offshore Wind Turbines. Diploma Thesis, National Technical University of Athens.

Liingaard, M., Andersen, L., Ibsen, L.B., 2007. Impedance of flexible suction caissons. Earthquake Engng Struct. Dyn 36(14), 2249 - 2271.

McCarron, W.O. and Sukumaran, B., 2000. Ultimate capacities of suction caissons and pile elements for deepwater applications. Proc. 10th International Offshore and Polar Engineering Conference, 2, pp. 466-469.

Mana, D.S.K., Gourvenec, S., and Randolph, M.F., 2014. Numerical Modeling of Seepage Beneath Skirted Foundations Subjected to Vertical Uplift. Comput Geotech, 55, 150–157.

Penzes, P., Jensen, M. R., Zania, V., 2016. Suction caissons subjected to monotonic combined loading. In Proceedings of the 17th Nordic Geotechnical Meeting.

Poulos, H.G., Davis, E.H., 1974. Elastic solutions for soil and rock mechanics. New York Wiley.

Randolph, M.F., O'Neill, M.P., Stewart, D.P. and Erbich, C., 1998. Performance of suction anchors in fine-grained calcareous soils. Proceedings of the 30th Offshore Technology Conference, Houston, Texas.

Raptakis, D., Chavez-Garcıa, F.J., Makra, K., Pitilakis, K., 2000. Site effects at EUROSEISTEST Part I. Determination of the valley structure and confrontation of observations with 1D analysis. Soil Dynam. Earthquake Engng 19(1), 1–22.

Senders, M., 2008. Suction Caissons in Sand as Tripod Foundations for Offshore Wind Turbines, PhD Thesis, University of Western Australia, Perth, Australia.

Senders, M., Kay, S., 2002. Geotechnical suction pile anchor design in deep water soft clays. Proceedings of Conference Deepwater Risers Mooring and Anchorings. The United Kingdom. London.

Skau, K.S., Chen, Y., Jostad, H.P., 2017. A numerical study of capacity and stiffness of circular skirted foundations in clay subjected to combined static and cyclic general loading. Géotechnique.

Sukumaran, B., McCarron, W.O., Jeanjean, P., Abouseeda, H., 1999. Efficient finite element techniques for limit analysis of suction caissons under lateral loads. Computers and Geotechnics, Volume 24(2), 89-107.

Supachawarote, C., Randolph, M., Gourvenec, S., 2004. Inclined Pull-out Capacity of Suction Caissons. Proceedings of the International Society of Offshore and Polar Engineers. France. Toulun.

Taiebat, H.A., Carter, J.P., 2000. Numerical studies of the bearing capacity of shallow foundations on cohesive soil subjected to combined loading. Geotechnique 50(4), 409-418.

Tsinidis, G., Pitilakis, K., Trikalioti, A.D., 2014. Numerical simulation of round robin numerical test on tunnels using a simplified kinematic hardening model. Acta Geotechnica 9(4), 641–659.

Ukritchon, B., Whittle, A.J. and Sloan, S.W., 1998. Undrained limit analyses for combined loading of strip footings on clay. J. Geotech. Geoenviron. Engng, ASCE 124(3), 265-276.

Vaschy, A., 1892. Sur les lois de similitude en physique, Annales Telegraphiques, 19, 25 28

Vulpe, C., 2015. Design method for the undrained capacity of skirted circular foundations under combined loading: effect of deformable soil plug. Géotechnique 65(8), 669–683.

Wroth, C.P., 1971.Some aspects of the elastic behaviour of overconsolidated clay. Proc Roscoe Memorial Symposium, 347-361.

Zafeirakos, A., 2014. Static and seismic inelastic response of deeply embedded foundations. PhD thesis, Laboratory of Soil Mechanics, National Technical University of Athens, Athens, Greece.

Zdravkovic, L., Potts, D.M., Jardine, R.J., 2001. A parametric study of the pull-out capacity of bucket foundations in soft clay. Geotechnique, 511, 55–67.

Zhu, B., Zhang, W.L., Ying, P.P. and Chen, Y.M., 2014. Deflection-based bearing capacity of suction caisson foundations of offshore wind turbines. ASCE J. Geotech. Geoenviron. Eng., 140(5): 04014033.

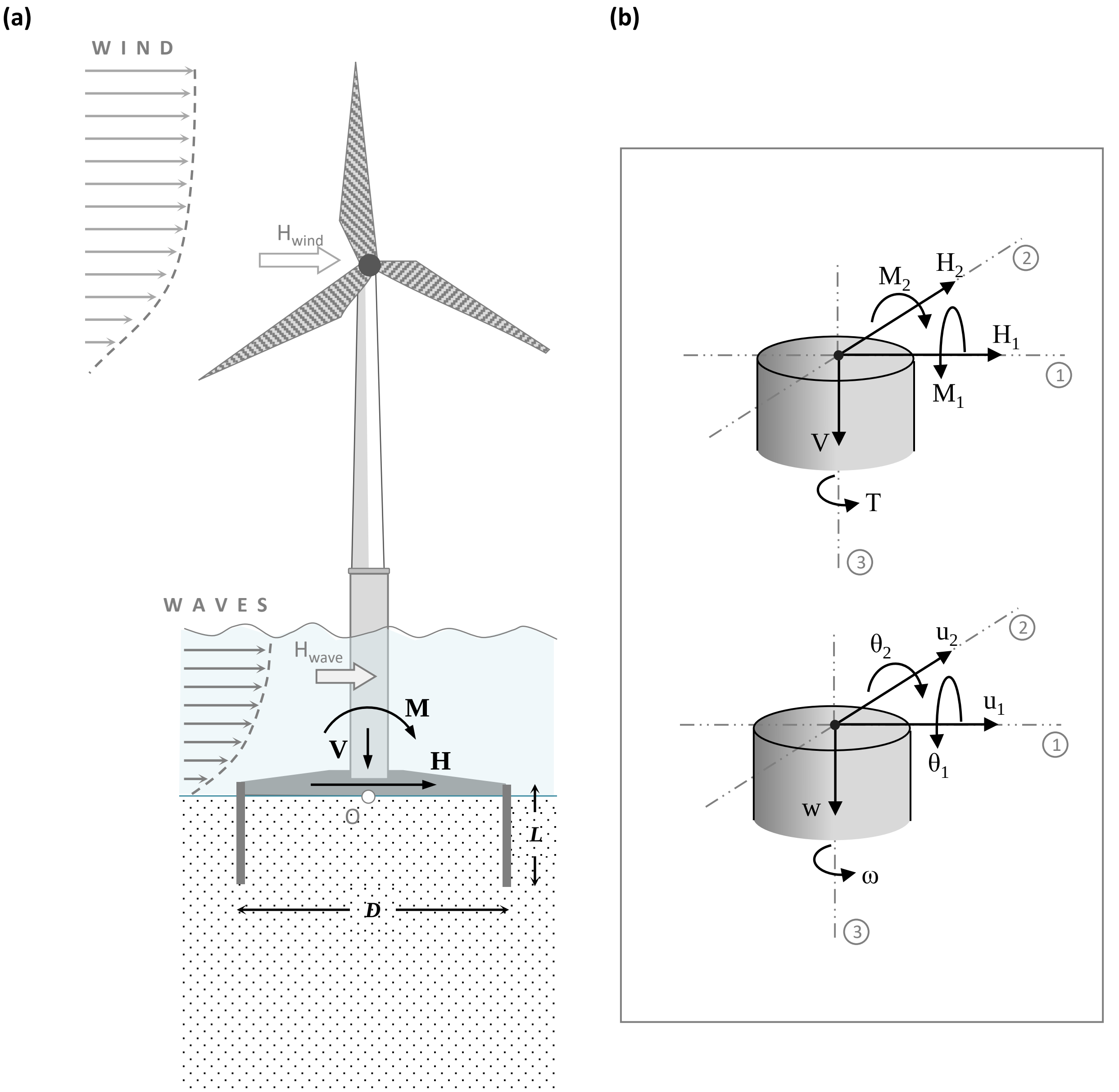

Figure 1. (a) A conceptual sketch of the problem under study: an offshore wind-turbine is founded on a suction caisson transmitting V-H-M loading at the top of the foundation; **(b)** nomenclature of generalized loads and corresponding caisson displacements.

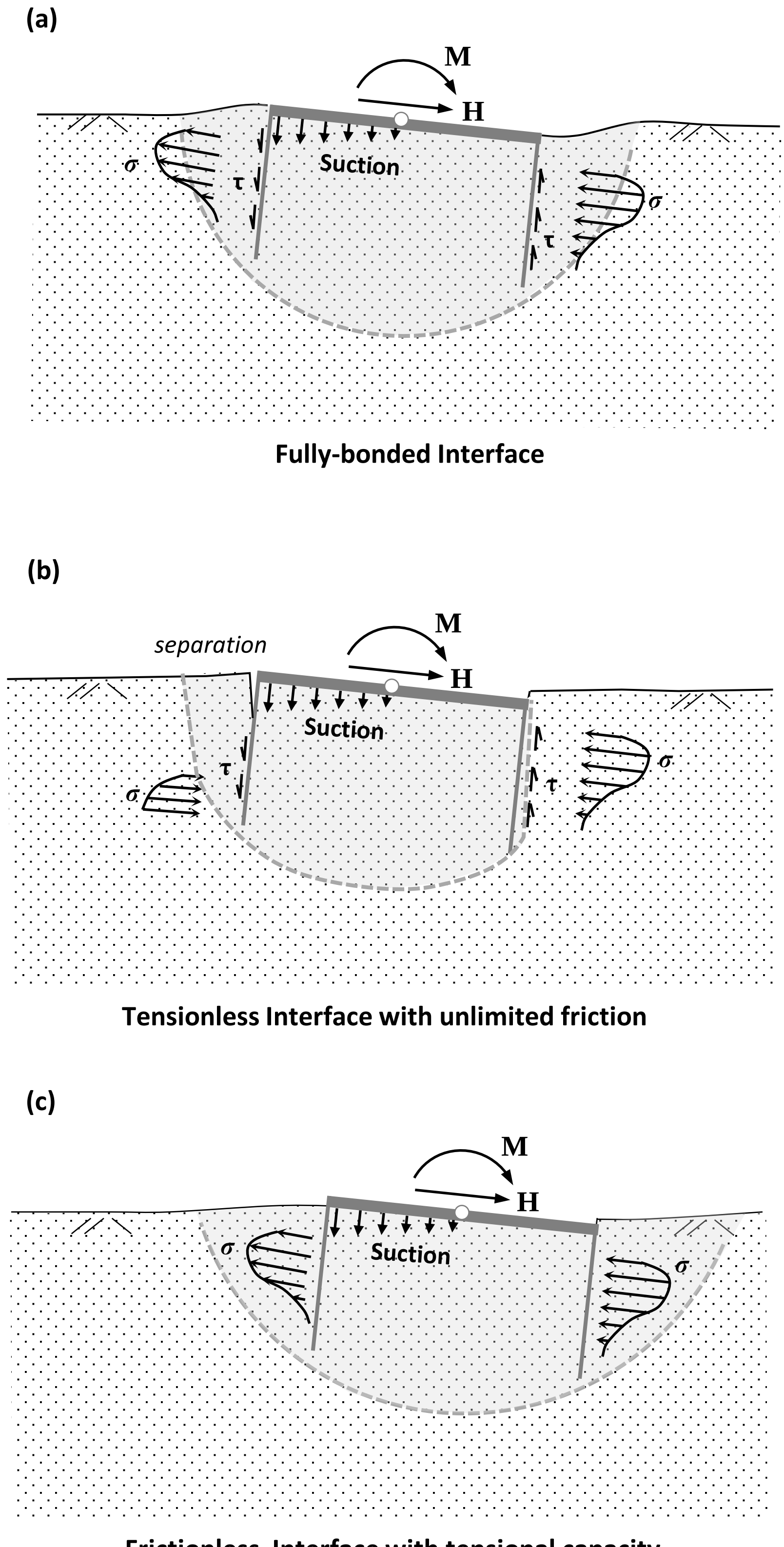

Figure 2. The three 'generic' interface scenarios: schematic representation of the bearing mechanism of a suction caisson subjected to combined H-M loading

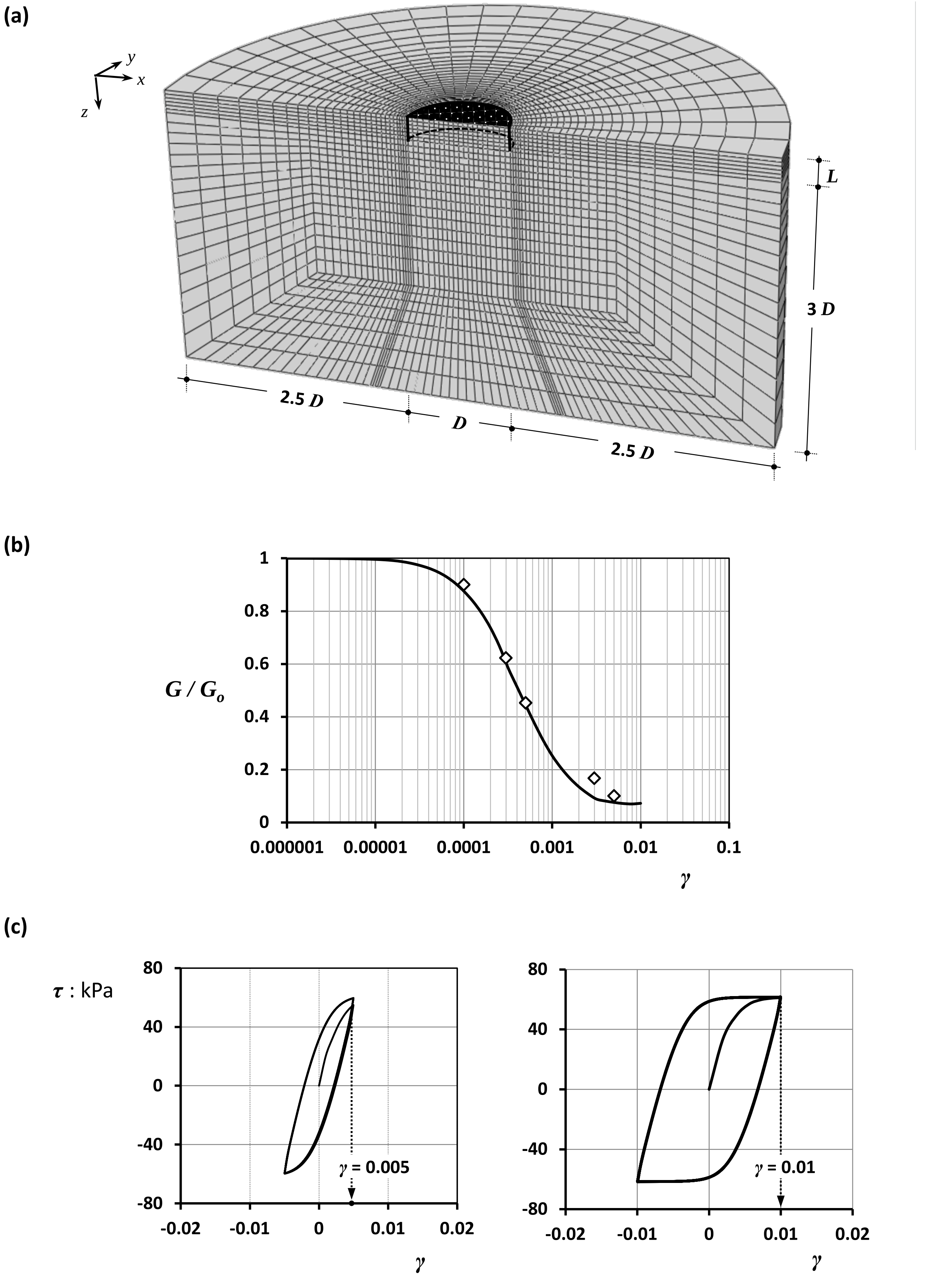

Figure 3. **(a)** A view of the semi-cylindrical finite element mesh for a caisson with L/D =0.2; **(b)** Comparison of G-γ curves produced utilizing the modified Von-Mises model (individual markers) described in this paper with the experimentally devired curve of Raptakis et al, 2000 (solid line); **(c)** Hysteresis τ-γ loops of a the example clay specimen (s_u *= 60 kPa,* E_{soil} *= 60000 kPa*) subjected to a cyclic simple shear quasi-static loading of 10 cycles at two characteristic stain levels: γ = 5 x 10^{-3} and γ =1x 10^{-2}.

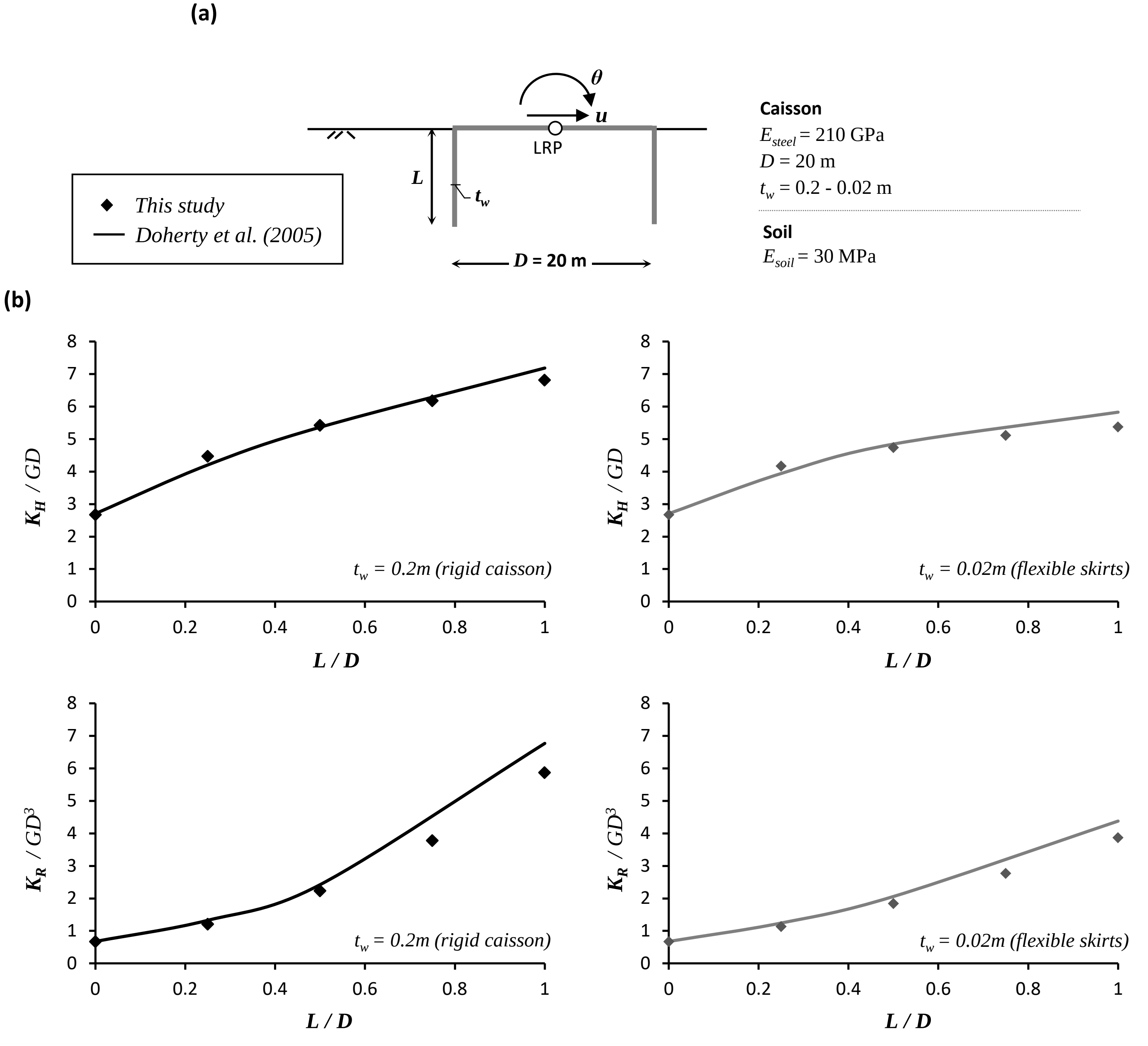

Figure 4. Elastic stiffnesses of caisson foundation embedded to elastic half-space: results from this study are compared to the results of Doherty et al (2005).

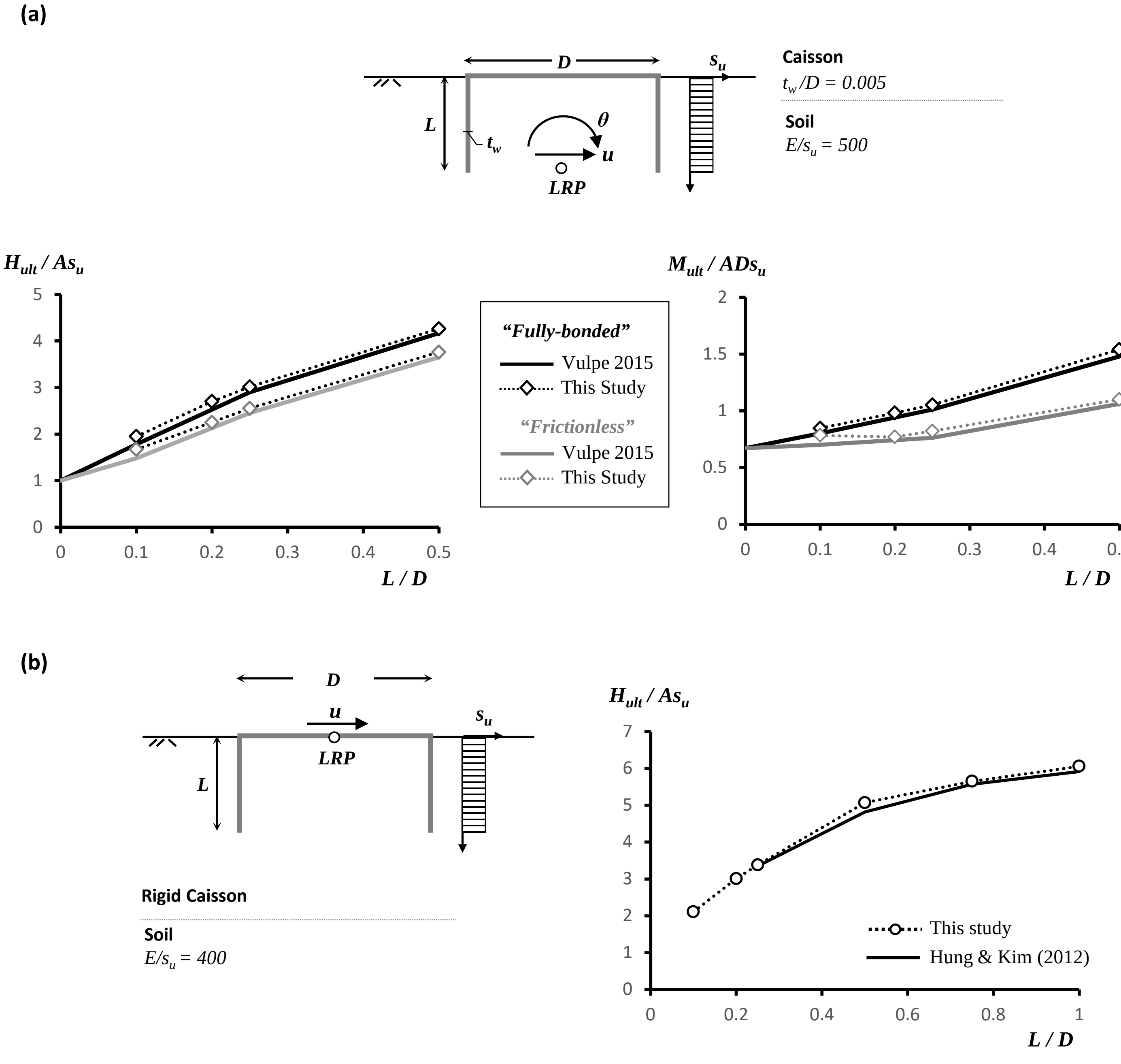

Figure 5. Capacity estimations of this study are validated against: **(a)** the study of Vulpe (2015) assuming Load Reference Point (LRP) at the base of the caisson and **(b**) the study of Hung & Kim (2012) assuming LRP at top lid and fully-bonded conditions.

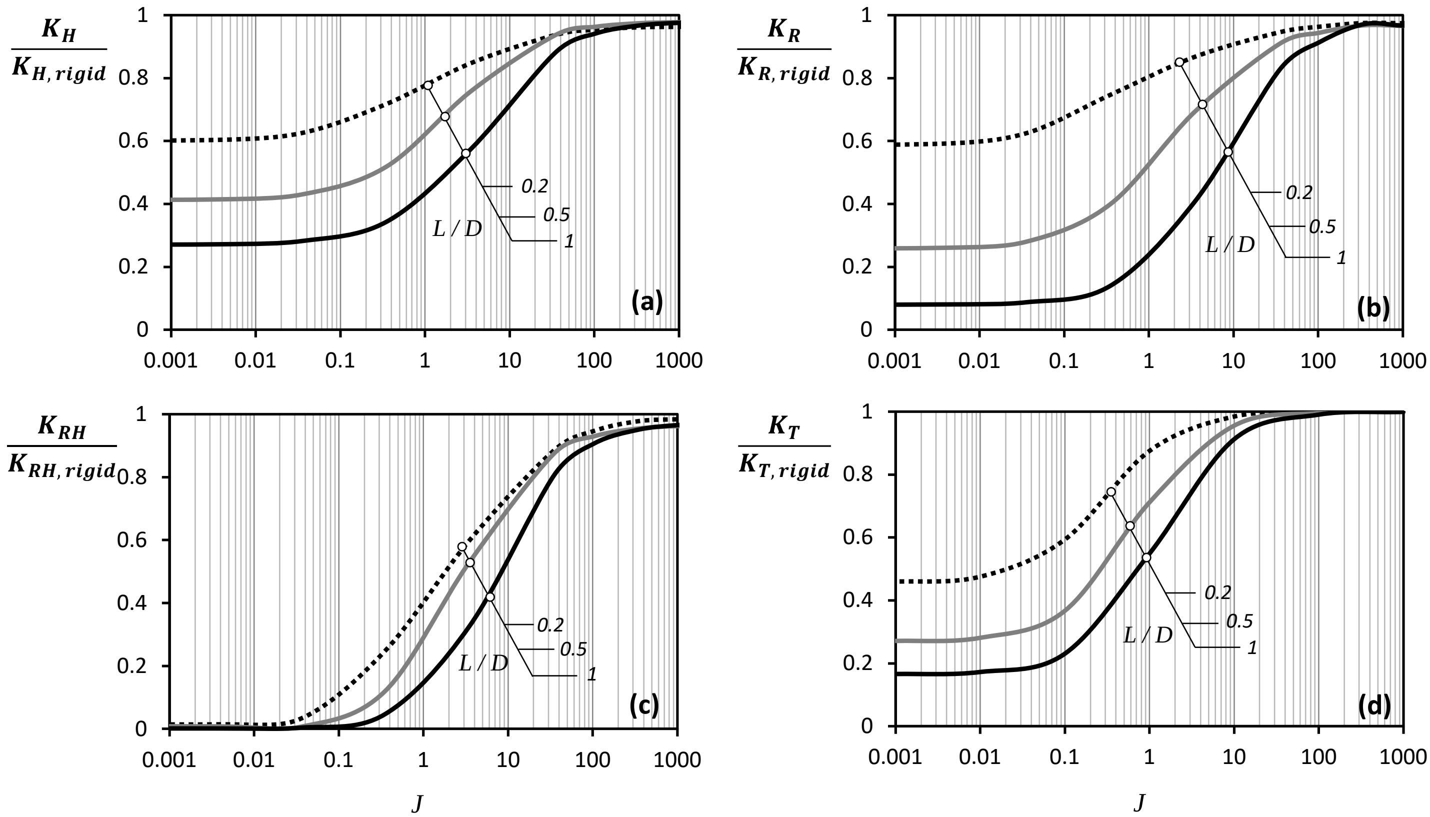

Figure 6. Ratios of the elastic stiffness of a skirted foundation "*fully-bonded*" to soil over the elastic stiffness of the equivalent rigid caisson as a function of embedment ratio L/D and skirt relative rigidity J : **(a)** horizontal; **(b)** rocking; **(c)** coupled swaying-rocking; **(d)** torsional stiffness.

(a)

Physical Variables

	D [m]	L [m]	E_{steel} [GPa]	t_w [m]	E_{soil} [MPa]	s_u [kPa]	γ' [kN/m^3]
Caisson 1	20	20	210	0.375	45	45	10
Caisson 2	10	10	210	0.25	60	60	10

Dimensionless Π-terms

	L/D	E_{soil}/s_u	J
Caisson 1	1	1000	875
Caisson 2	1	1000	875

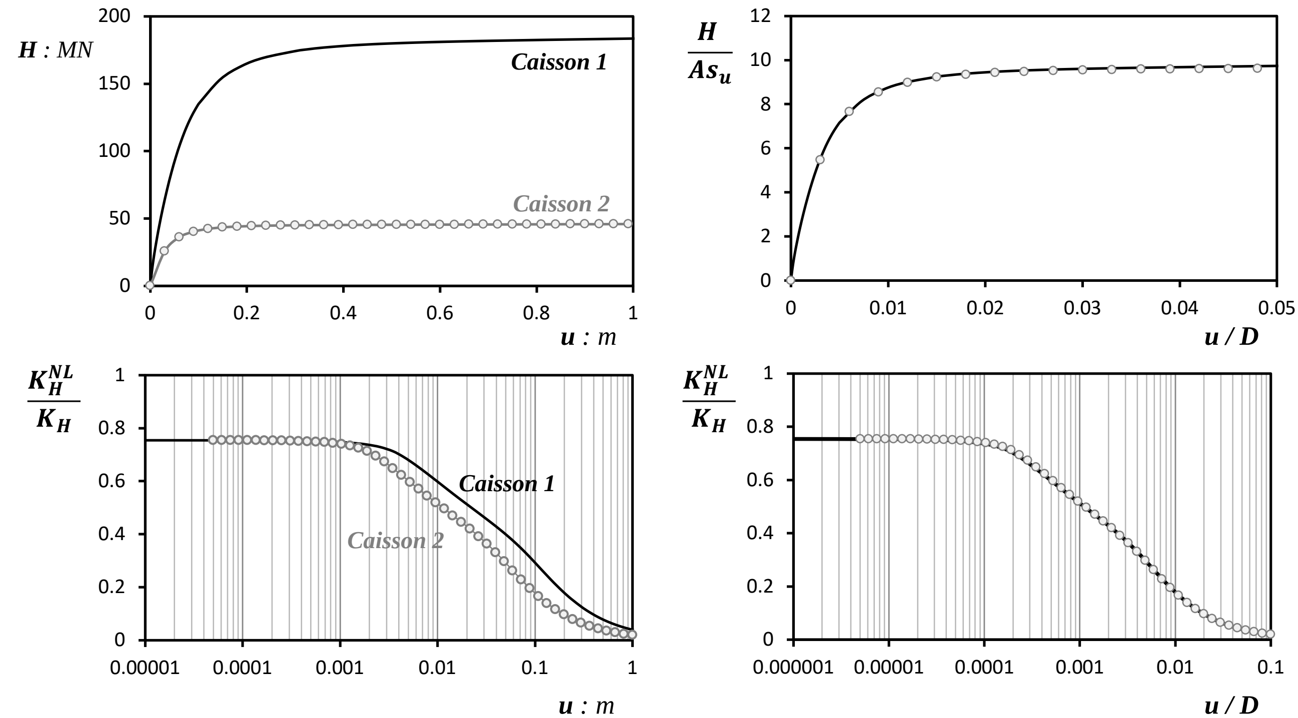

(b)

Physical Variables

	D [m]	L [m]	E_{steel} [GPa]	t_w [m]	E_{soil} [MPa]	s_u [kPa]	γ' [kN/m^3]
Caisson 1	20	20	210	1	240	240	10
Caisson 2	10	10	210	0.25	120	120	10

Dimensionless Π-terms

	L/D	E_{soil}/s_u	J	$s_u/\gamma' L$
Caisson 1	1	1000	437.5	1.2
Caisson 2	1	1000	437.5	1.2

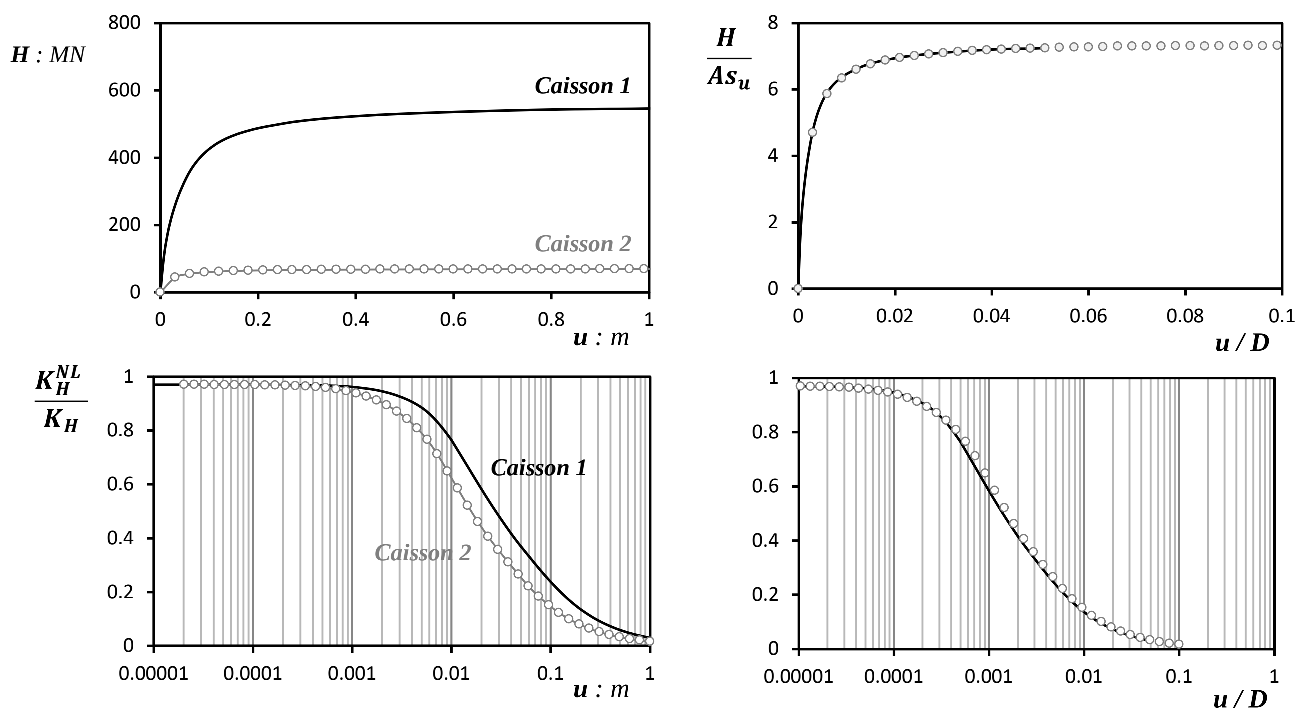

Figure 7. Formulation of the dimensionless load-carrying response of a suction caisson in a yielding uniform clay stratum: application to **(a)** 'frictionless 'and **(b)** tensionless interface conditions

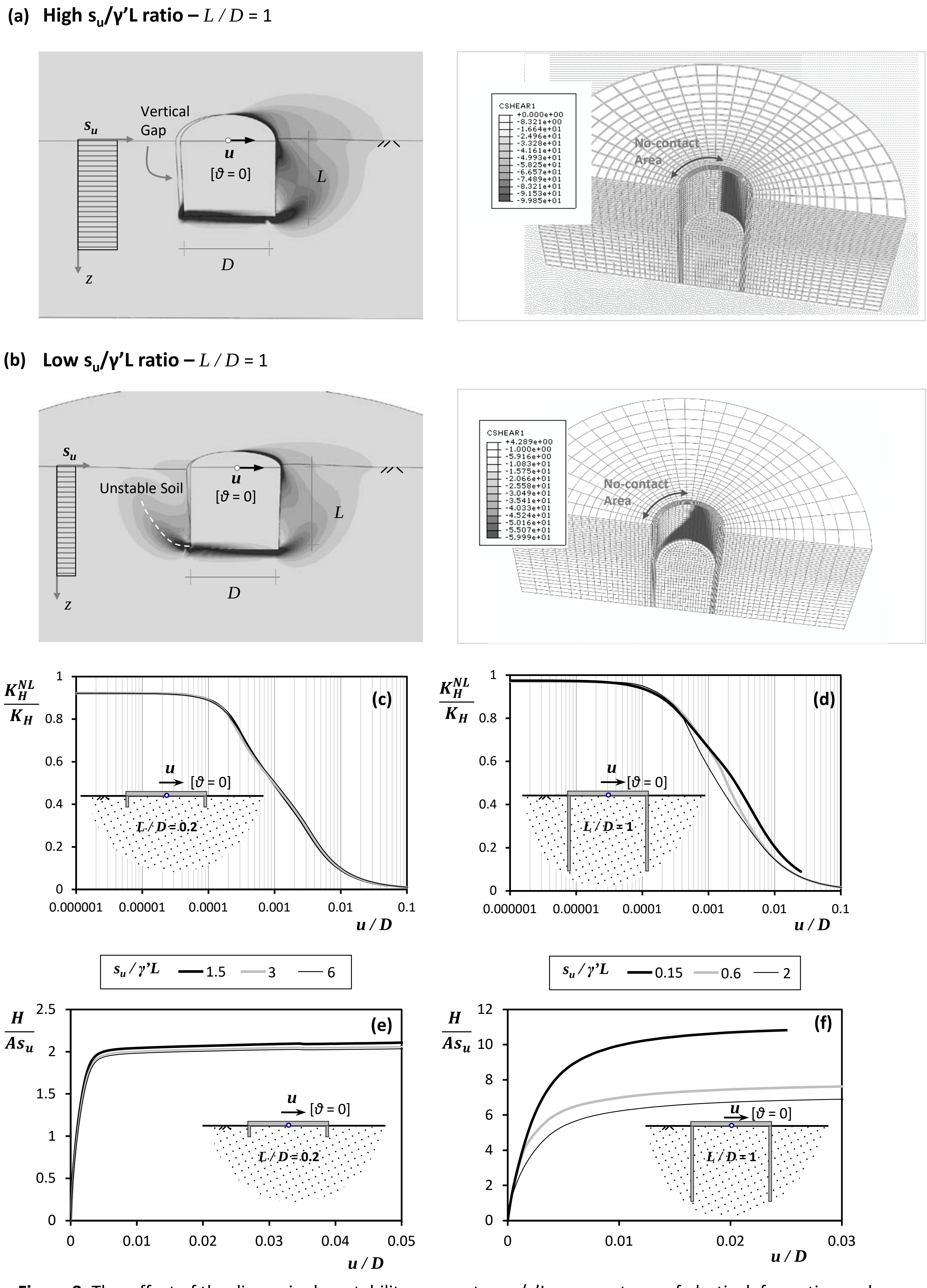

Figure 8. The effect of the dimensionless stability parameter $s_u/\gamma' L$ on : contours of plastic deformation and contours of shear stressing along the caisson skirts for caissons with **(a)** high and **(b)** low stability parameter; on the dimensionless stiffness **(c,d)** and capacity **(e,f)** of shallow and deep caissons.

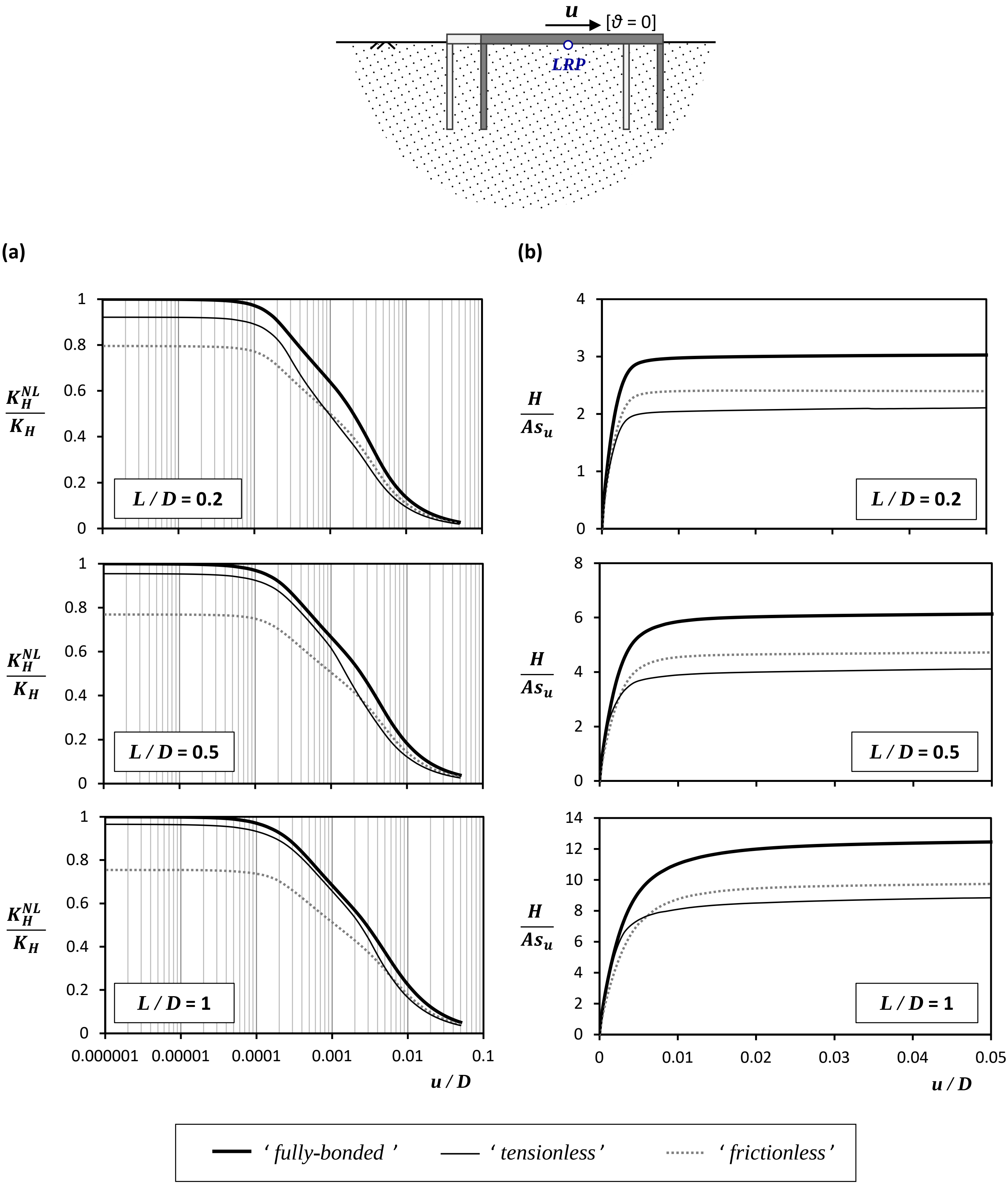

Figure 9. Effect of soil nonlinearity and interface conditions on : **(a)** the horizontal stiffness K_H and **(b)** the dimensionless lateral capacity H of a rigid skirted foundation with plan view A, diameter D, and embedment depth L. In all interface scenarios results refer to uniform soil of E_{soil} / s_u = 1000. Results for the tensionless interface have been derived for stability factors $s_u / \gamma' L = 1.5$ (for L/D = 0.2), $s_u / \gamma' L$ = 0.6 (for L/D =0.5) and $s_u / \gamma' L$ = 0.3 (for L/D = 1)

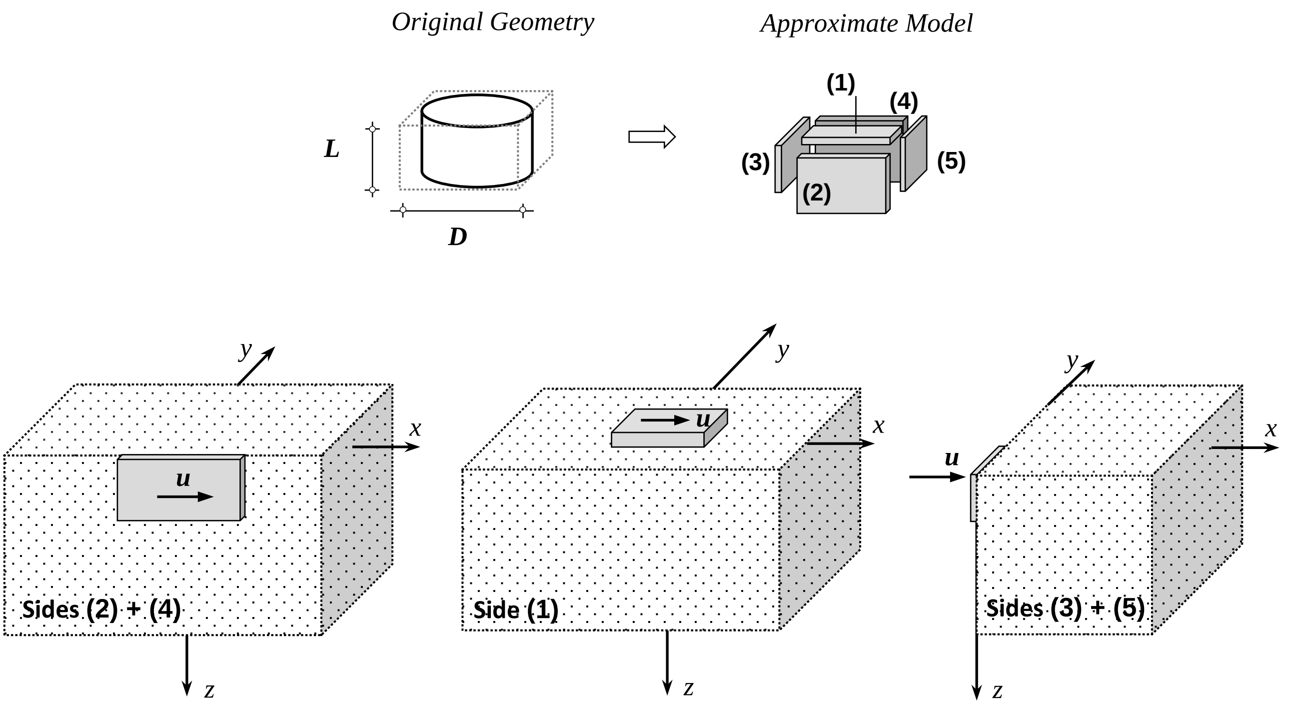

Figure 10. Definition of the "Approximate Model" and schematic view of the contribution of each side on the total foundation stiffness : application to horizontal stiffness

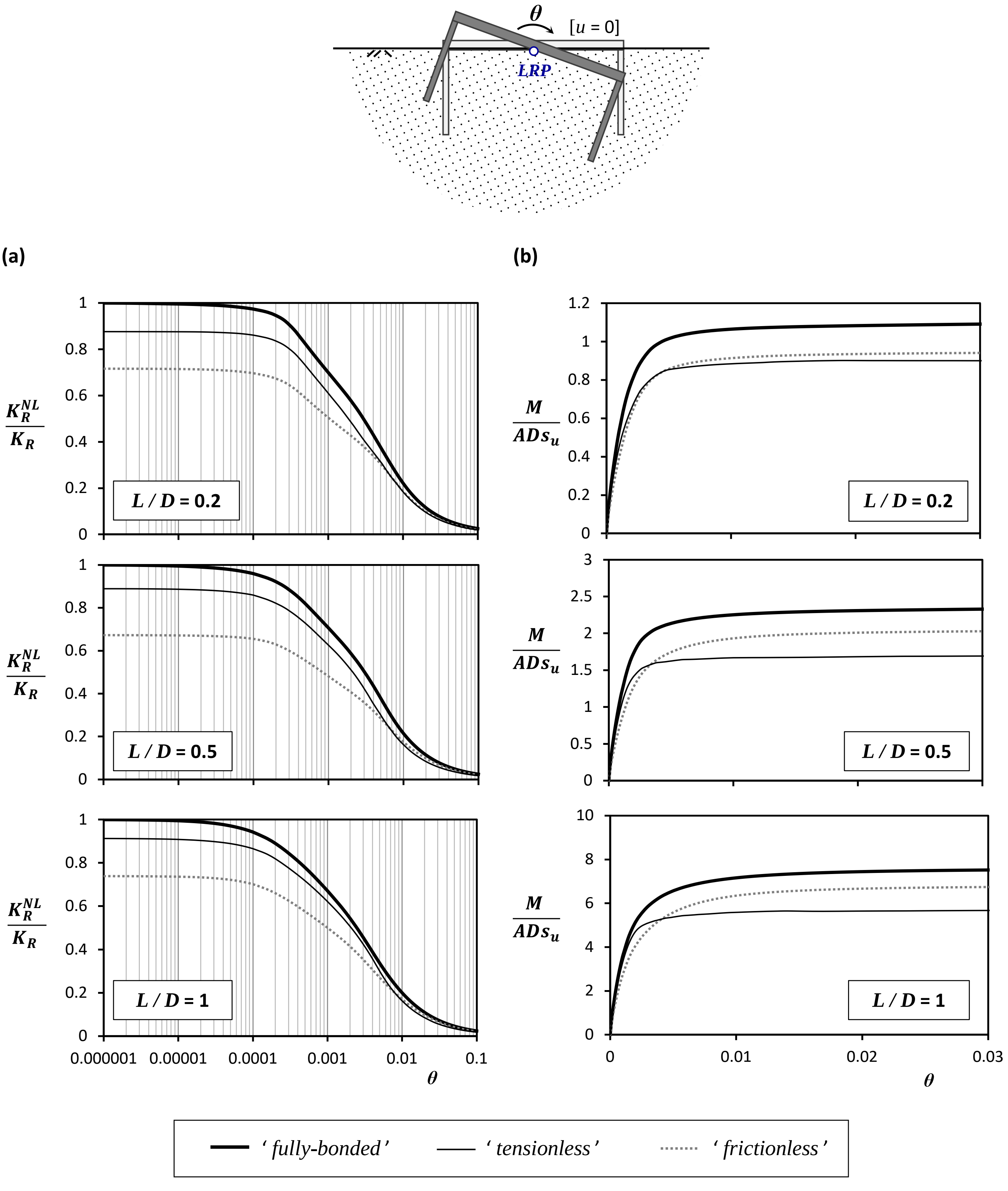

Figure 11. Effect of soil nonlinearity and interface conditions on : **(a)** the Rotational stiffness K_R and **(b)** the overturning capacity M (expressed in dimensionless terms) of a rigid skirted foundation with a plan view A, diameter D, and embedment depth L. In all interface scenarios results refer to uniform soil of E_{soil} / s_u = 1000. Results for the tensionless interface have been derived for stability factors $s_u / \gamma' L = 1.5$ (for L/D = 0.2), $s_u / \gamma' L$ = 0.6 (for L/D =0.5) and $s_u / \gamma' L$ = 0.3 (for L/D = 1)

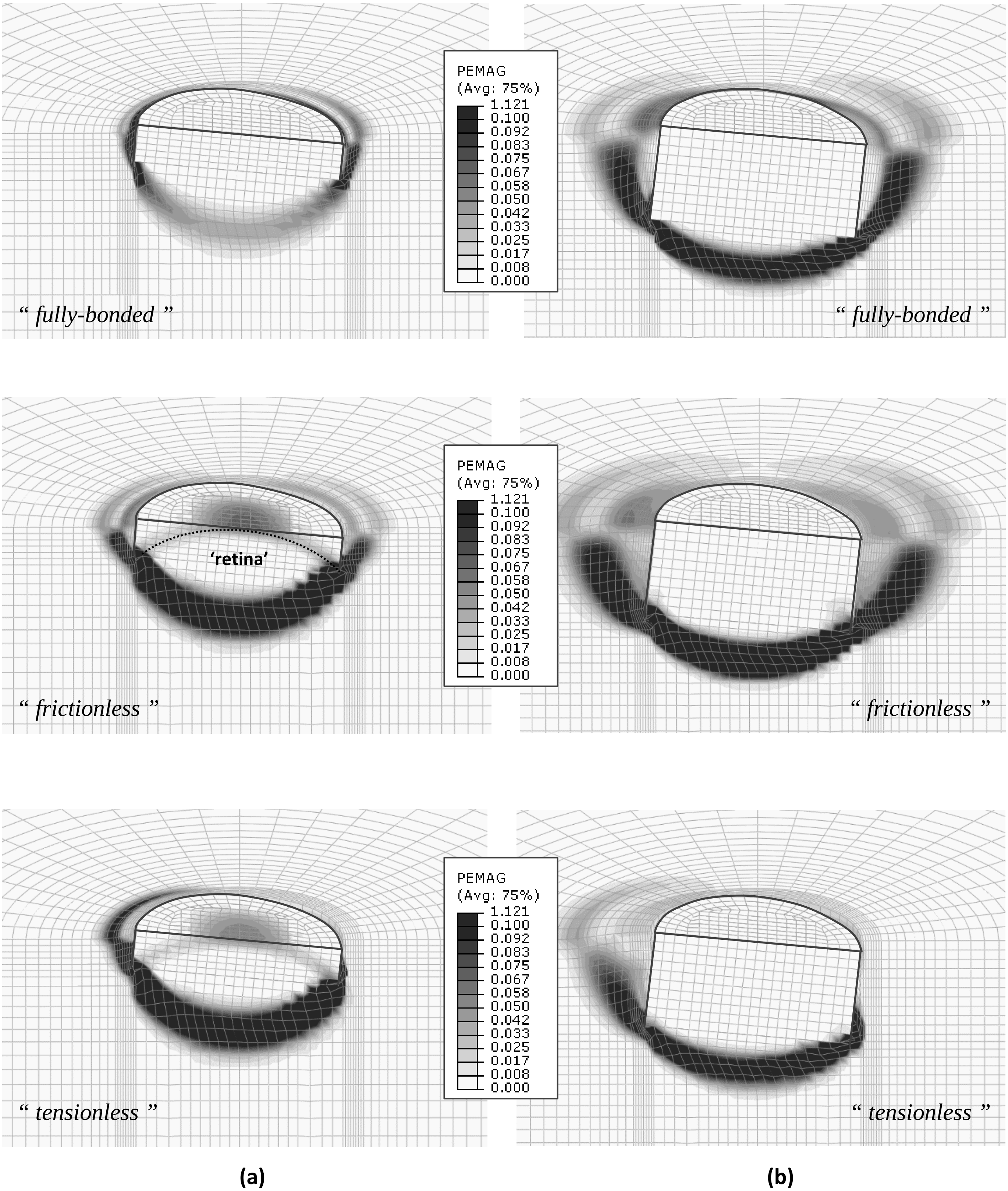

Figure 12. Effect of interface conditions on the rotational bearing mechanism of a skirted footing with (a) $L\,/\,D$ = 0.2 and (b) $L\,/\,D$ = 0.5.

(a)

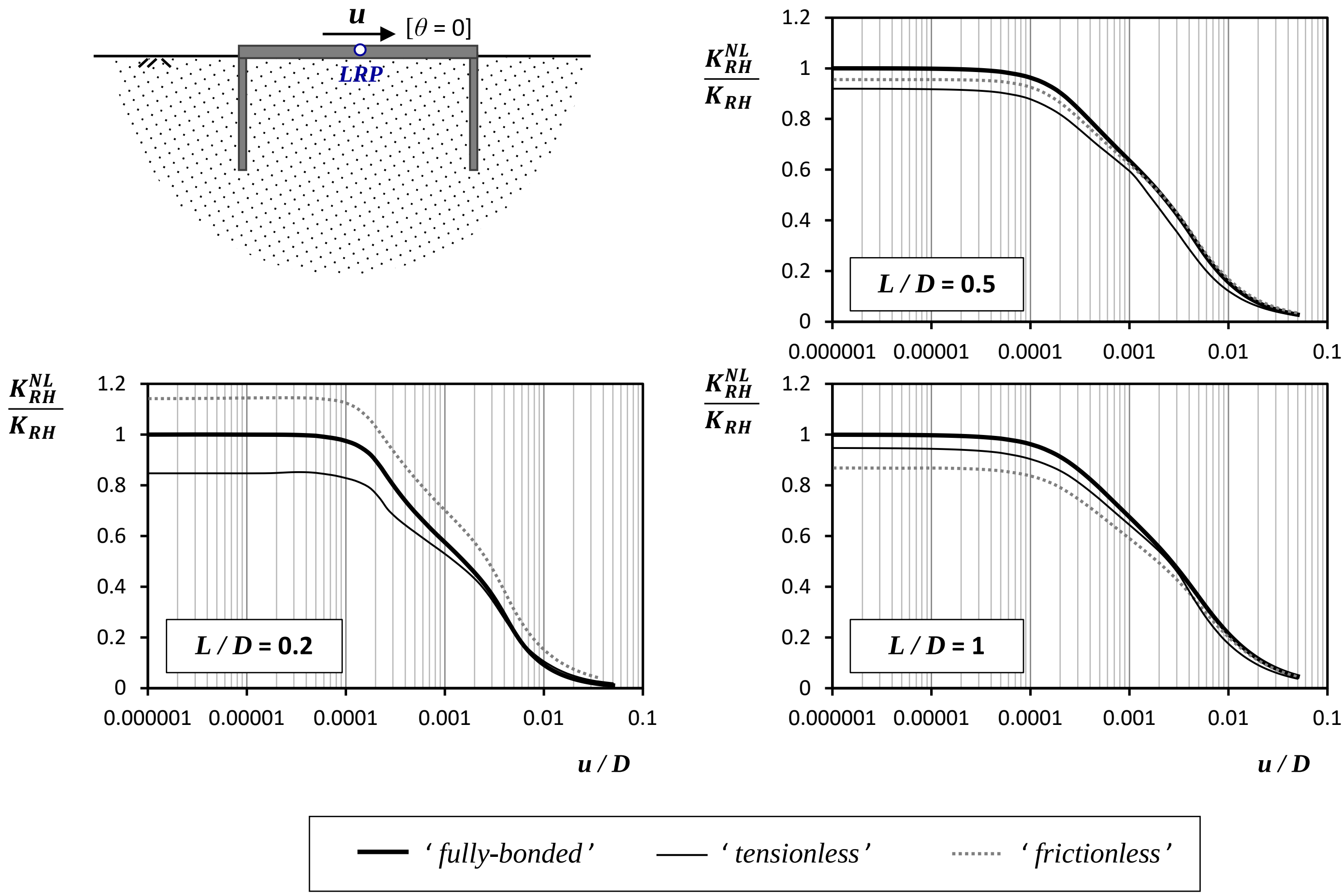

Figure 13. Effect of soil nonlinearity and interface conditions on the coupled swaying-rocking stiffness K_{RH}^{NL} of a rigid skirted foundation with a plan view A, diameter D, and embedment depth L. In all interface scenarios results refer to uniform soil of E_{soil} / s_u = 1000. Results for the tensionless interface have been derived for stability factors $s_u / \gamma' L$ = 1.5 (for L/D = 0.2), $s_u / \gamma' L$ = 0.6 (for L/D =0.5) and $s_u / \gamma' L$ = 0.3 (for L/D = 1)

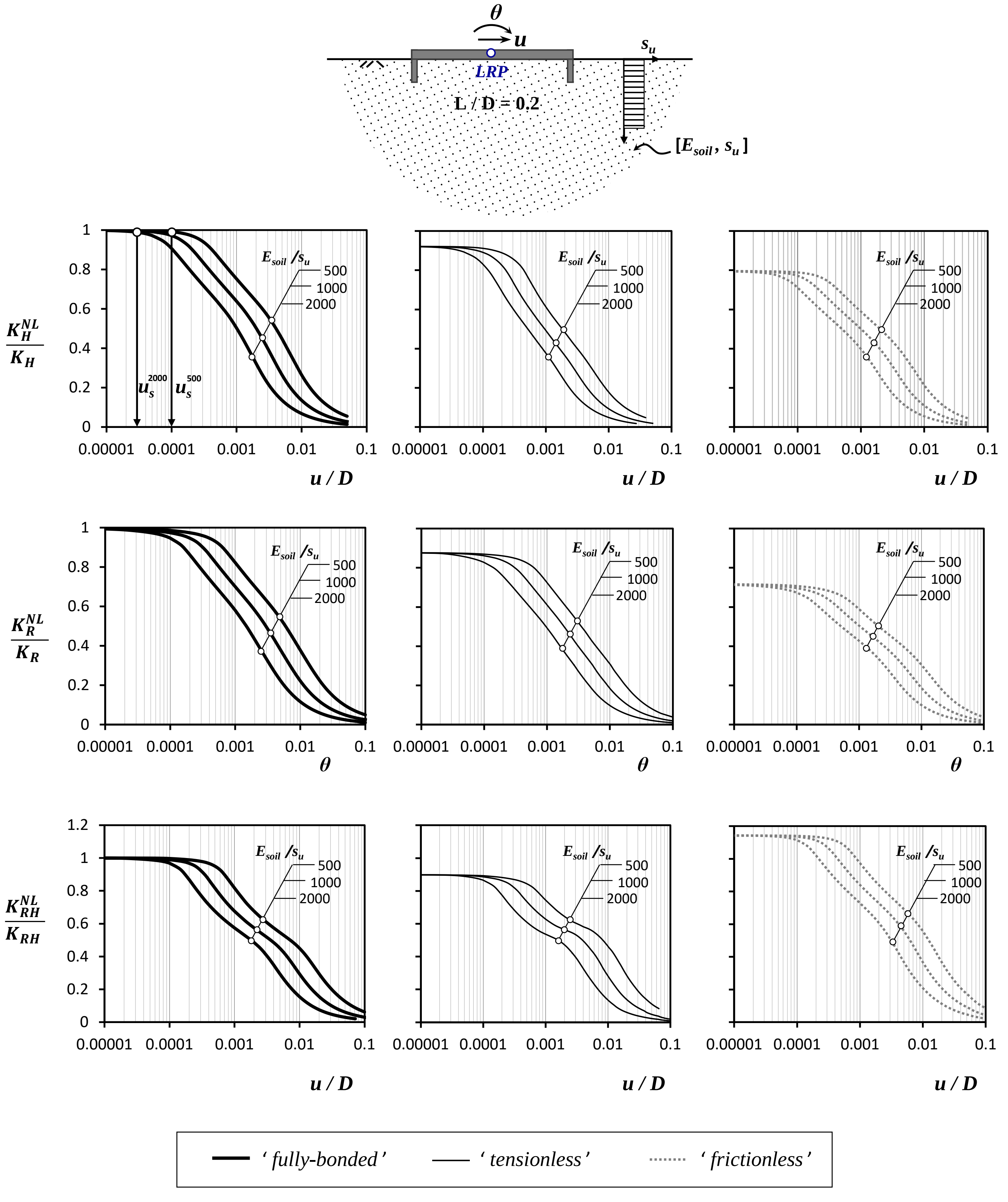

Figure 14. Nonlinear stiffnesses of a rigid skirted foundation with embedment ratio L/D = 0.2: The combined effect of soil rigidity index (E_{soil} /s_u) and interface conditions. Results for the 'tensionless' interface assumption refer to stability factor s_u / $\gamma' L$ = 1.5.

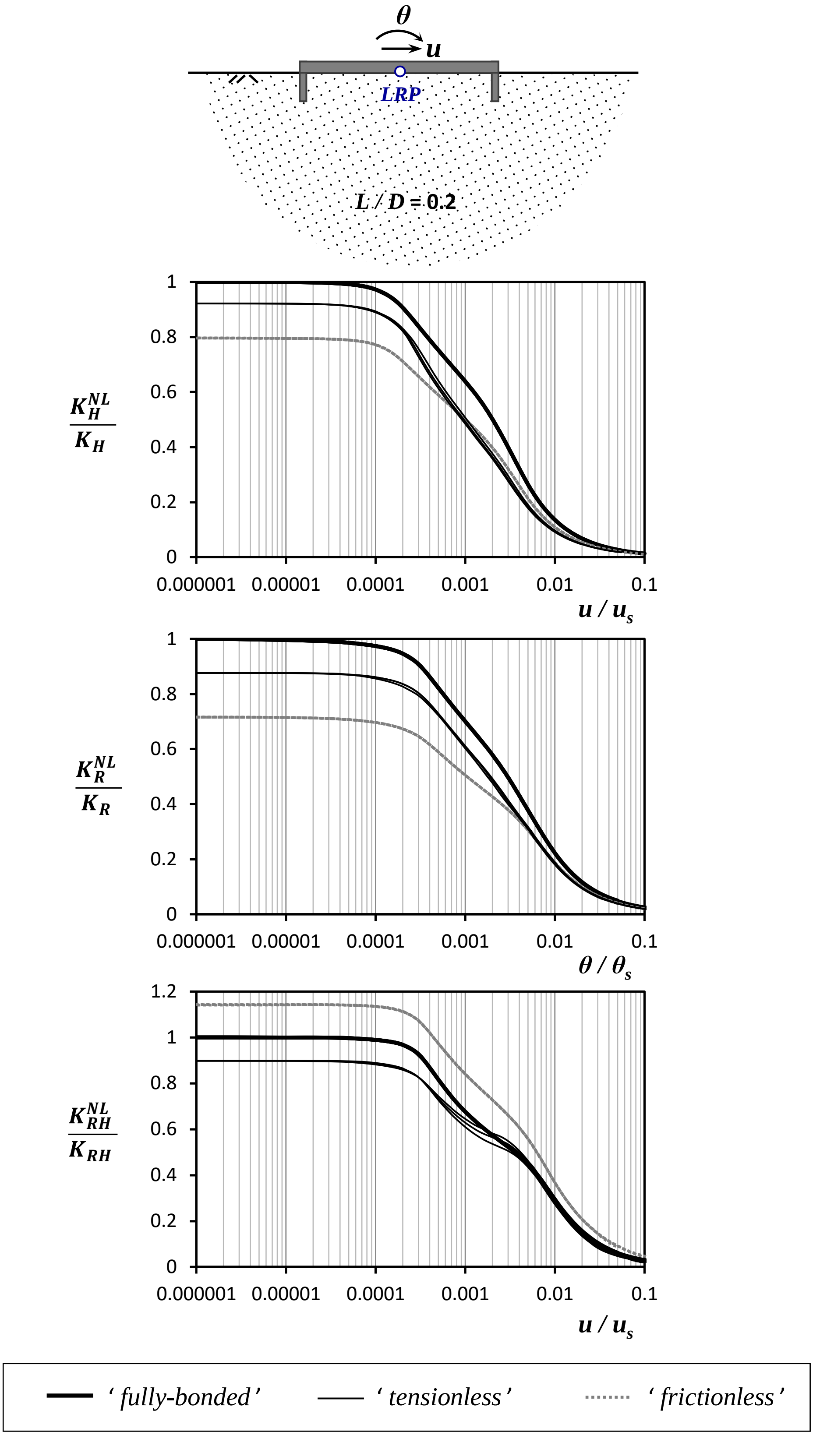

Figure 15. Nonlinear stiffnesses of a rigid skirted foundation with embedment ratio L/D = 0.2 expressed in terms of the dimensional quantity u / u_s or θ / θ_s.

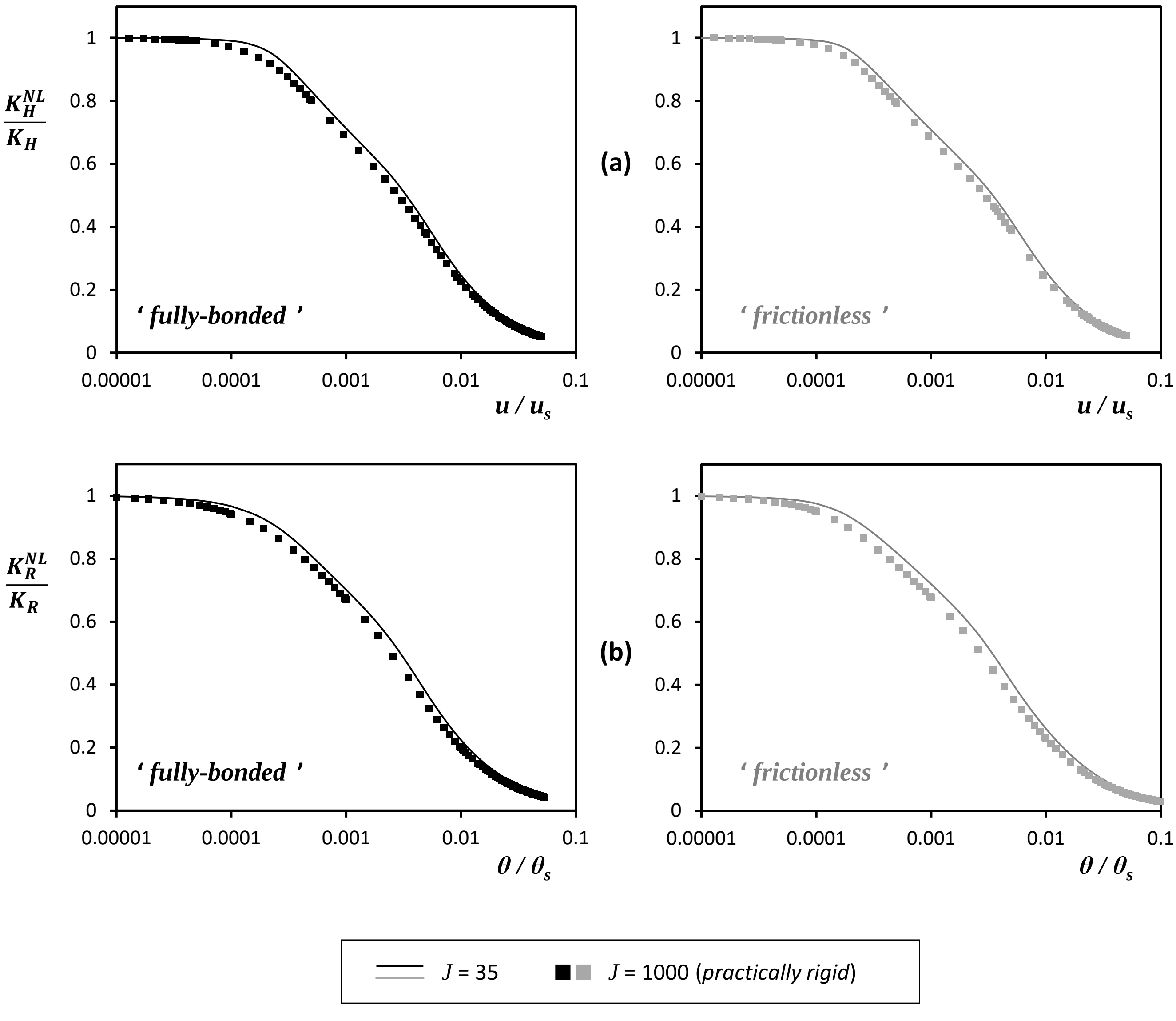

Figure 16. Comparison between a practically rigid (J = 1000) and a flexible (J = 35) caisson with L/D = 1 in terms of nonlinear stiffness K^{NL} : **(a)** horizontal; **(b)** rotational stiffness, assuming *fully-bonded* (left) and *frictionless* interfaces (right).

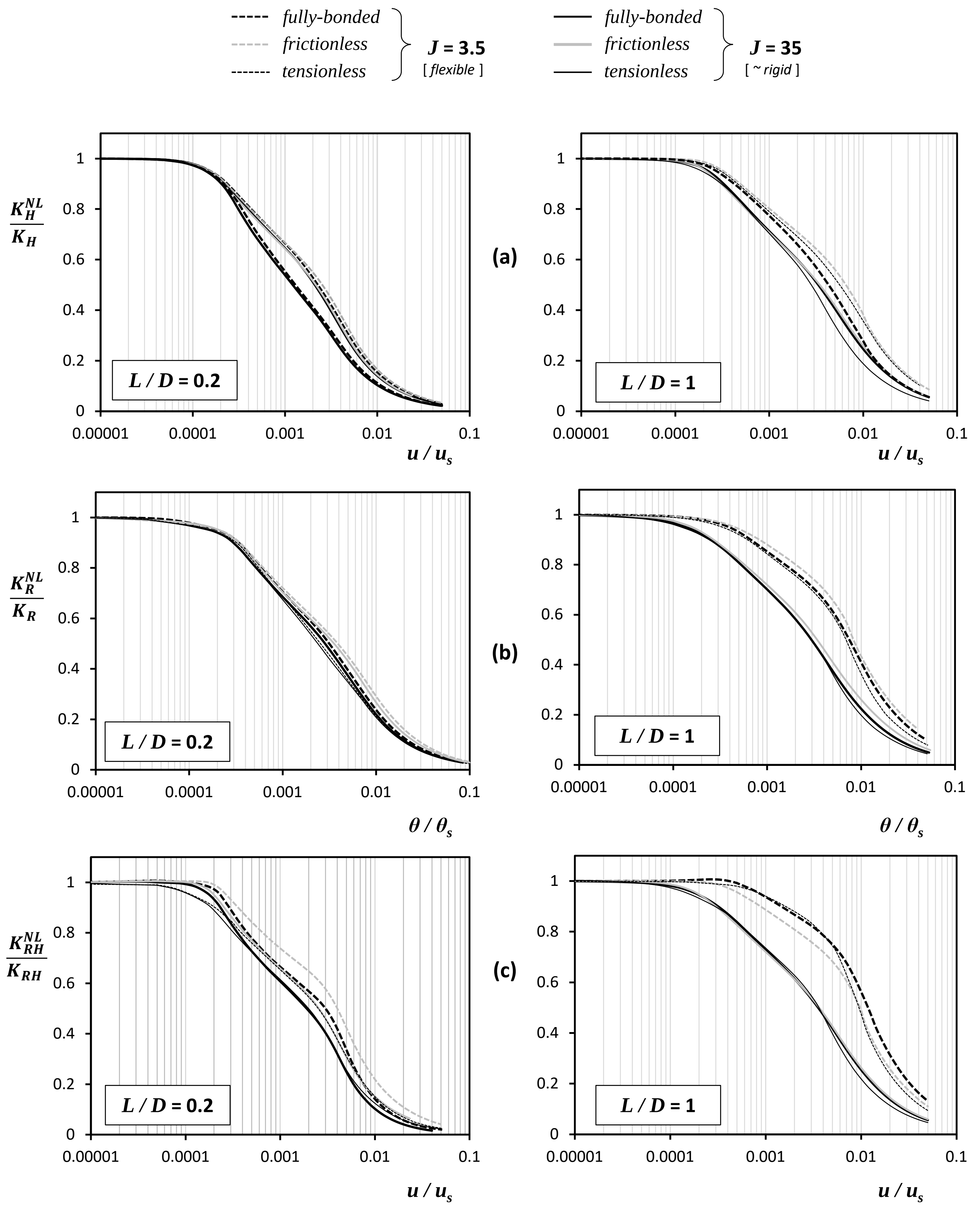

Figure 17. Effect of skirt relative rigidity J on the nonlinear stiffness K^{NL} of a shallow (L/D = 0.2) and a deep (L/D = 1) caisson : **(a)** horizontal ; **(b)** rotational ; **(c)** coupled swaying-rocking stiffnesses. The tensionless curves (thin black line) have been derived assuming for the shallow caisson a $s_u / \gamma' L$ = 1.5 and for the deeper caisson $s_u / \gamma' L$ = 0.3.

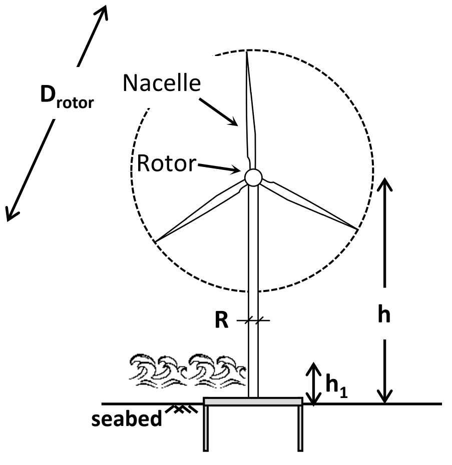

Table 1. Dimensions and loads of an example 3.5 MW offshore wind-turbine tower.

Tower Properties				
$\mathbf{D_{rotor}}$: m	**Nacelle + Rotor Mass** : t_n	**h** : m	$\mathbf{h_1}$: m	**R** : m
90	220	80	20	2

ULS Loads	
Wind Load: kN	**Wave Load:** kN
1.5	2.5

Table 2a. Performance assessment of suction caissons at ULS conditions assuming *'fully-bonded'* interface.

	Effective Stiffness K			*Foundation Rotation*				*Foundation Displacement*			
Iter. No	K_H : kN/m	K_R : kNm/rad	K_{HR} : kN/rad	θ_s	θ : mrad	θ/θ_s	Error: $\Delta\theta/\theta$	u_s	u :m	u/u_s	Error: $\Delta u/u$
				Caisson 1 : [D = 20 m | L/D = 0.2]							
-	1653595	166342398	3649842	1	0.97	0.97	-	20	0.0046	0.00023	-
1	1488235	117271391	2627886	1	1.35	1.35	38.9%	20	0.0051	0.00025	11.1%
2	1455164	106459135	2445394	1	1.48	1.48	9.8%	20	0.0052	0.00026	3.3%
3	1451856	104795711	2408896	1	**1.50**	1.50	1.5%	20	**0.0053**	0.00026	0.2%
				Caisson 2 : [D = 12 m | L/D = 1]							
-	1526051	182897051	9763034	1	1.42	0.00142	-	12	0.0117	0.00097	-
1	1098756	117054113	6785308	1	2.26	0.00226	59.4%	12	0.0176	0.00147	50.5%
2	984303	100593378	5857820	1	2.57	0.00257	13.7%	12	0.0193	0.00161	10.0%
3	961412	96935437	5740664	1	**2.70**	0.00270	5.0%	12	**0.0203**	0.00169	4.7%

Table 2b. Performance assessment of suction caissons at ULS conditions assuming *'frictionless'* interface.

	Effective Stiffness K			*Foundation Rotation*				*Foundation Displacement*			
Iter. No	K_H : kN/m	K_R : kNm/rad	K_{HR} : kN/rad	θ_s	θ : mrad	θ/θ_s	Error: $\Delta\theta/\theta$	u_s	u : m	u/u_s	Error : $\Delta u/u$
				Caisson 1 : [D = 20 m | L/D = 0.2]							
-	1322876	119766527	4160820	1	1.48	0.00148	-	20	0.0077	0.00038	-
1	1058301	77848242	3079007	1	2.27	0.00227	53.9%	20	0.0104	0.00052	35.5%
2	1018614	69464585	2829357	1	2.53	0.00253	11.4%	20	0.0110	0.00055	5.5%
3	1005386	68266920	2787749	1	**2.58**	0.00258	1.8%	20	**0.0111**	0.00056	1.5%
				Caisson 2 : [D = 12 m | L/D = 1]							
-	1144538	135343818	8493839	1	2.42	0.00242	-	12	0.021	0.00179	-
1	709614	75792538	5011365	1	4.29	0.00429	77.5%	12	0.036	0.00299	67.7%
2	597449	60227999	4077043	1	5.32	0.00532	24.0%	12	0.043	0.00358	19.6%
3	566546	53731496	3711808	1	**5.82**	0.00582	9.5%	12	**0.045**	0.00377	5.2%